Geochemistry, Geophysics, Geosystems®

AGU ADVANCING EARTH AND SPACE SCIENCE

RESEARCH ARTICLE
10.1029/2022GC010657

The Meaning of Pressure for Primary Magmas: New Insights From PRIMELT3-P

Claude T. Herzberg[1], Paul D. Asimow[2], and Juan David Hernández-Montenegro[2]

[1]Earth and Planetary Sciences, Rutgers University, Piscataway, NJ, USA, [2]Geological and Planetary Sciences, California Institute of Technology, Pasadena, CA, USA

Key Points:

- New software is reported for computing the pressure and temperature at which a primary basaltic magma was formed in the mantle
- The meaning of magmatic pressure in the mantle source is examined with Hawai'i and Iceland as test cases
- Pressures reflect magma segregation and mixing in melt channels, with minima that coincide with geophysically constrained boundary layers

Supporting Information:

Supporting Information may be found in the online version of this article.

Correspondence to:

C. T. Herzberg,
herzberg@eps.rutgers.edu

Citation:

Herzberg, C. T., Asimow, P. D., & Hernández-Montenegro, J. D. (2023). The meaning of pressure for primary magmas: New insights from PRIMELT3-P. *Geochemistry, Geophysics, Geosystems*, *24*, e2022GC010657. https://doi.org/10.1029/2022GC010657

Received 11 AUG 2022
Accepted 16 DEC 2022

Author Contributions:

Conceptualization: Claude T. Herzberg, Paul D. Asimow
Data curation: Claude T. Herzberg
Formal analysis: Claude T. Herzberg, Paul D. Asimow
Investigation: Claude T. Herzberg, Paul D. Asimow
Methodology: Claude T. Herzberg, Paul D. Asimow
Project Administration: Claude T. Herzberg
Resources: Claude T. Herzberg

Abstract This paper reports new software, PRIMELT3-P, for computing the pressure and temperature range over which a primary basaltic magma was formed by adiabatic decompression and fractional melting of fertile mantle peridotite. The underlying model was developed to explore the meaning of magmatic pressure and its connection to the physics of mantle melting, melt extraction, and melt migration. We present a comparison of the results of the batch melting model FractionatePT3 (Lee et al., 2009, https://doi.org/10.1016/j.epsl.2008.12.020) and the new fractional melting model PRIMELT3-P, each applied to basalts from various localities, with a particular focus on Hawai'i and Iceland. The unexpected result is that pressures for batch melting and fractional melting are quite similar across a broad range of potential temperatures, agreeing to within ±0.29 GPa (1σ) when applied to magmas that pass tests for derivation from peridotite sources. Although samples from both Hawai'i and Iceland yield a range of final pressures of melting, the minimum final pressure in each location coincides with independent geophysical constraints—the depth to the lithosphere-asthenosphere boundary beneath Hawai'i and to the Moho below Iceland. These results clarify the meaning of primary magma pressure, but the concept remains complex. We suggest that computed temperature and pressure arrays arising from heterogeneous peridotite-source primary magmas may reflect melt transport and mixing in a thermally zoned mantle plume with a complex network of branching melt channels that nucleate over a range of depths.

Plain Language Summary Partial melting of the Earth's mantle yields primary basaltic magmas that segregate from their residues, ascend to the surface, typically cool and evolve at shallow levels, and then erupt at volcanic provinces. The melting may take place over a range of temperatures and pressures and may involve open-system processes that are difficult to reproduce directly in laboratory experiments. Hence it remains a challenging problem to determine the range of pressures over which a particular lava sample was generated. Here we report new software, PRIMELT3-P, that adds estimates of the pressure range of melt generation to information of earlier versions of the software. Results show that the range of samples from particular volcanic provinces (such as Hawai'i and Iceland) can yield a substantial range of pressures of melting, possibly indicating variability in the mechanisms of melt migration with the mantle melting regime. The minimum pressures observed in each place correlate with geophysical estimates of the depths to boundaries that might arrest the melting process, such as the base of the lithosphere or the crust. Both PRIMELT3-P and the geobarometer of Lee et al. (2009, https://doi.org/10.1016/j.epsl.2008.12.020; FractionatePT3) are calibrated for peridotite sources and fail when applied to melts extracted from pyroxenite sources.

1. Introduction

The modeling approach and associated software PRIMELT3 (Herzberg & Asimow, 2015) were designed to invert primitive basalt compositions for the primary magma composition, the 1 atm olivine liquidus temperature of the primary magma, and the mantle potential temperature at which the primary magma would be generated by batch or accumulated fractional melting of peridotite. Its successor PRIMELT3-P has the same strengths and limitations. It is restricted to primitive basalts that differ from their primary magmas only due to olivine addition or subtraction; this excludes most basalts, which have generally also fractionated plagioclase and clinopyroxene. Successful solutions are only possible for primary magmas derived from a nominally anhydrous fertile peridotite source, not from pyroxenite or from volatile-rich peridotite sources. Each of these restrictions has been documented in detail (Herzberg & Asimow, 2008, 2015) and the software provides tests and flags that recognize and warn the user when the model is being misapplied.

Software: Claude T. Herzberg, Paul D. Asimow, Juan David Hernández-Montenegro
Validation: Claude T. Herzberg
Writing – original draft: Claude T. Herzberg
Writing – review & editing: Claude T. Herzberg, Paul D. Asimow, Juan David Hernández-Montenegro

The goal of PRIMELT3-P is to add estimation of the pressure of melt generation to the primary magma solution. There is a history of attempts to carry out similar estimates of pressure of melting with various approaches. The wide divergence among early efforts (e.g., O'Hara, 1968; Presnall et al., 1979) was primarily the result of widely differing assumptions and methods for calculating the primary magma compositions associated with observed, evolved magmas. The first generation of magmatic pressure models was based on the decrease, with increasing pressure, in the activity of SiO_2 in basaltic melts coexisting with olivine and orthopyroxene (Albarède, 1992; Haase, 1996). These were later recalibrated by Putirka (2008) and Lee et al. (2009) using larger experimental databases. Despite different formulations of the activity-composition relationship for SiO_2 in the melt, the Putirka (2008) and Lee et al. (2009) calibrations recover experimental batch melting pressures to within ±0.29 and ± 0.20 GPa 1σ, respectively. As this paper is not intended to be a review of different barometers, it is sufficient for us to compare pressures obtained from PRIMELT3-P with those obtained from one of these similar models; we choose the FractionatePT3 software of Lee et al. (2009).

An important question that arises is what, exactly, do we mean by a primary magma pressure? Lee et al. (2009) state: "*the primary magma represents the aggregate of many melt increments generated along a polybaric melting path, and thus the P and T of this primary magma is taken to represent the weighted average P and T of the melting path (assuming no shallow-level re-equilibration) or, alternatively, the P and T of shallow-level re-equilibration in the mantle*." But the idea of an "average" pressure is difficult to reconcile with the wide range of temperatures and pressures calculated for various samples from a given locality (for Hawai'i, e.g., 1.5–6.0 GPa and 1400–1700°C; Figure 2b in Lee et al., 2009). Another source of confusion is that models that make a primary magma by the aggregation of small melt droplet. along a polybaric melting path do so by fractional melting (e.g., Asimow et al., 2001; Herzberg & O'Hara, 2002; Kinzler, 1997; Langmuir et al., 1992). But the Lee et al. (2009) method is strictly based on batch (or equilibrium) melting because it is calibrated directly from experimental data. This is not merely a semantic distinction because analytical solutions to the equations for batch and accumulated fractional melting (Shaw, 1970) yield different primary magma compositions. For example, primary magmas of accumulated fractional melting are higher in FeO and lower in SiO_2 at constant MgO content and melt fraction (Herzberg, 2004; Herzberg & O'Hara, 2002; Langmuir et al., 1992); they also have a more restricted range of CaO contents (Herzberg, 2006, 2011). Asimow and Longhi (2004) showed that, essentially by coincidence, the accumulated primary melts generated by decompression melting of typical fertile upper mantle sources at typical modern terrestrial potential temperatures can be quite close to possible batch melts of the same source, and that the pressure implied by applying a batch melting paradigm to the accumulated fractional melt is generally near the middle of the range of pressures of fractional melt generation. But it is unclear in what sense this is an average pressure of melt extraction and how the average is weighted. Krein et al. (2021) interpreted this result to mean that fractional melting does not matter and that the primary magma problem can be solved for batch melting and applied with confidence, but this is a misinterpretation of the conclusion of Asimow and Longhi (2004); while an accumulated fractional melt may be roughly consistent with being a batch melt of the same source, that does not imply that it is the *right* batch melt to represent the average of the fractional melting process. Moreover, a batch melting solution to the primary magma problem yields no insight into questions concerning the *range* of pressures over which melting may have taken place.

Batch melting is thought to occur when a partial melt in the mantle remains in equilibrium with its residue at any melt fraction and in a closed system of constant bulk composition until there is a single separation event. In its purest form, the prediction of batch melting is the formation of one primary magma composition with a magmatic pressure that represents only the pressure at the melt segregation event, having no memory of processes that occurred at lower extents of melting. In a batch melting context, variations in magmatic pressure among samples from a given locality represent a range in the pressure of melt segregation events and are insensitive to variations in source composition and potential temperature.

The physics of fractional melting is different. It may occur when partial melts drain from their sources by buoyant porous flow and matrix compaction at low melt fractions during decompression (Ahern & Turcotte, 1979; McKenzie, 1984), if the migrating melts do not undergo further equilibration with residues as they migrate. Mixing of such melts produces an accumulated fractional melt. This protracted process may leave a specific residue, such as lherzolite or harzburgite, at the end of melt production, but the mixed melt is never in equilibrium with it; only the final drop of liquid extracted is in equilibrium with the residue (Asimow & Longhi, 2004; Herzberg, 2004). However, counterintuitively, mass balance is achieved between the residue and the accumulated fractional melt, not the final drop of melt (Herzberg, 2004). PRIMELT3-P calculates the composition of the

polybaric accumulated fractional melt. Unlike batch melting, the aggregate melt composition can only be simulated computationally (Herzberg & O'Hara, 2002; Langmuir et al., 1992) as its experimental determination in the laboratory is not practical (Asimow & Longhi, 2004).

We explore the problem of what the pressure of batch melting means by comparison with magmatic pressures obtained for accumulated fractional melting. To do so, we apply both FractionatePT3 and PRIMELT3-P to primary magma compositions from a variety of occurrences. We focus special attention on Hawai'i and Iceland as test cases because magmatic pressures can be compared with geophysically constrained depths to the lithosphere-asthenosphere boundary and to the seismic Moho, respectively. We offer new insights on the compromising effects of lithological variability on magmatic pressures and temperatures; both FractionatePT3 and PRIMELT3-P have been calibrated on peridotite melting experiments that are not always relevant to residues of pyroxenite melting. Finally, we show that there can be significant primary magma heterogeneity arising from the melting of mantle peridotite; preservation of this heterogeneity in the erupted lava sequence is interpreted to reflect melt transport in channels.

2. Method

2.1. A Fractional Decompression Melting Model

To understand the meaning of magmatic pressure and how it is computed in the fractional melting model, we briefly review the method and its assumptions (Herzberg & O'Hara, 2002). A simulated decompression fractional melting process begins at an initial pressure P_i. The theoretically continuous process of formation and extraction of infinitesimal melt increments is approximated by discrete steps in which a quantity of melt corresponding to a mass fraction of 0.01 of the (declining) residue mass is generated, its composition is calculated with Shaw's (1970) batch melting equation, and it is isolated from the residue. The removal of each instantaneous melt increment changes the composition and mass of each successive residue, causing an increase in the distribution coefficient of MgO between the residue and liquid (i.e., $D_{MgO,in}$ of Herzberg & O'Hara, 2002) with decompression. This was calibrated from experiments on fertile peridotite KR-4003 (Walter, 1998) and its parameterization (Herzberg & O'Hara, 2002), permitting a calculation of pressure for each instantaneous melt droplet along an adiabatic gradient that begins at P_i. The process is repeated continuously along a vertical streamline until melting stops at a final melting pressure P_f. Each increment of extracted liquid is mixed with the previously formed melt to form an accumulated fractional melt. The integration of the incremental melts into the accumulated melt, which is weighted only by melt mass extracted along a one-dimensional streamline and hence is most applicable to a columnar rather than triangular melting regime, keeps track of the mass of liquid and residue as fractions of the initial source mass. This total mass fraction of liquid is known in the model as F_{AFM}, and solutions are analytically identical to F in Shaw's (1970) equation for accumulated fractional melting. This is a "forward" polybaric decompression melting model. Based on parameterizations of distribution coefficients as functions of the MgO content of the residues, solutions to Shaw's (1970) equation for batch melting were obtained for the SiO_2, Al_2O_3, FeO, MgO and CaO contents of the incremental melts which were mixed to yield compositions of the accumulated fractional melts and their residues at each F_{AFM} and final melting pressure P_f (Herzberg & O'Hara, 2002; Table A2; Herzberg, 2004, Appendix 1 and Table A2). It is important to recognize that the pressure decrement required to yield a 1% increase in melt fraction is neither assumed a priori (as in models such as Langmuir et al. (1992)) nor derived from a conservation of entropy criterion (as in MELTS-based models such as Asimow et al. (2001)).

Descriptions of how PRIMELT3 software combines this "forward" calculation with an "inverse" calculation of olivine addition or subtraction to compute a primary accumulated fractional melt composition corresponding to a given observed melt composition were given earlier (Herzberg & Asimow, 2015; Herzberg & O'Hara, 2002). An example is given again in Figure S1 in Supporting Information S1. Briefly, an olivine control line though an observed primitive lava composition is generated by incremental addition or subtraction of the equilibrium olivine composition, producing an array of potential primary magma compositions. For each point on this array, F is calculated in normative Ol-An-Qz (projected from Di) space and F_{AFM} in an FeO-MgO diagram (Figure 1). The fields and melt fractions in Ol-An-Qz were mostly constrained by fitting Walter's experimental data on KR-4003, except that F for residual harzburgite was calculated from Shaw's equation for batch melting. By using Shaw's (1970) equation for accumulated fractional melting it can be demonstrated that melt fraction contours for residual harzburgite in Ol-An-Qz space are distributed similarly to those for batch melting, and this approximation

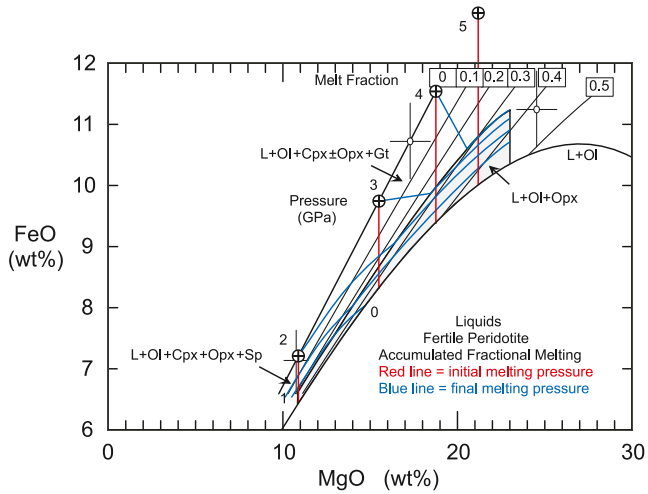

Figure 1. A binary MgO-FeO projection of primary magma compositions formed by accumulated fractional melting of fertile peridotite KR-4003, modified from Herzberg and Asimow (2008). Red and blue lines are initial melting pressure P_i and final melting pressure P_f, respectively, encoded in PRIMELT3-P. Brackets show the 1σ uncertainty in the Fe-Mg distribution coefficient between olivine and melt in high pressure experiments (Herzberg & O'Hara, 2002). PRIMELT3 solutions are restricted to primary magmas having MgO < 23.0%.

has little effect on primary magma calculations. Olivine addition increases the estimated melt fractions in both these diagrams, but at different rates. Each 1% olivine increases F_{AFM} in the FeO-MgO diagram substantially more than it increases F in normative Ol-An-Qz space. PRIMELT3 is therefore able to identify a unique primary magma composition from among the family of potential primary magma compositions by locating the point where a common melt fraction arises in both diagrams, as shown in Figures S1a and S1b in Supporting Information S1. This is a mass balance solution to the primary magma problem, given an assumed peridotite composition. The model is most accurate if the source composition is similar to the KR-4003 xenolith bulk composition used in Walter's (1998) experiments, upon which it is calibrated. Although results can be obtained that account to first order for variable source compositions, wildly different sources (such as Martian mantle compositions) require recalibration of the melt fraction contours in Ol-An-Qz space.

Herein we consider how a primary magma solution in FeO-MgO space, with a known value of F_{AFM}, defines initial and final melting pressures P_i and P_f. In principle, they can be read off figures such as Figure 1, but we seek a parameterization that can yield more precise results with less effort. The first such parameterization was given in Herzberg and Gazel (2009) for the purpose of modeling the Galapagos mantle plume. In that study, melting pressures were parameterized as functions of primary magma FeO and MgO content. Results were restricted to pressures <3.0 GPa, and the effects of residual source lithology were not explored. In the present study we expand the pressure range to 7 GPa. At elevated pressures, FeO-MgO-P_f systematics are more dependent on residuum mineralogy (Figure 1) and a more complex parameterization is required than that provided by Herzberg and Gazel (2009).

2.2. Parameterization of P_i and P_f

Here we develop a method that calculates final melting pressure P_f from the combination of initial melting pressure P_i and the pressure extent of the melting column, dP:

$$dP \equiv P_i - P_f \tag{1}$$

Primary magma MgO contents change little during decompression (Figure 7a; Herzberg & Asimow, 2015), and we assume they are constant (Figure 1) and related to initial pressure of melting. In this model, there is a good fit for initial pressure (in GPa) versus the MgO content (in weight percent) of the first liquid along the anhydrous peridotite solidus from 2.5 to 7 GPa using:

$$P_i = 11.248\,\mathrm{MgO} - 13700\,\mathrm{MgO}^{-2} - 8.13\,(\ln(\mathrm{MgO}))^2 \tag{2}$$

(Herzberg & Gazel, 2009). However, it is restricted to fertile peridotite with garnet as the primary aluminous phase on the solidus, and so applies only for $P_i \geq 2.5$ GPa (Klemme & O'Neill, 2000; Longhi, 2002) and MgO contents ≥12.3 wt.%. In this paper we extend it to lower pressures by recalibrating to more accurately reflect the shape of the solidus of spinel peridotite and by incorporating different calibrations of melt productivity for different residual mineralogies.

Herzberg and Asimow (2015) offered an update to Equation 2 intended for extension to lower pressures and MgO content, as needed for modeling spinel lherzolite melting below oceanic ridges. They combined a new parameterization of the solidus in P-T space with a fit to the MgO contents of liquids coexisting with fertile peridotite as a function of P and T. The solidus of Herzberg and Asimow (2015), their Equation 15, included a deep cusp at the plagioclase-spinel lherzolite transition at 1 GPa, at which the MgO content of the solidus liquid drops to 4 wt.%. However, pMELTS (Ghiorso et al., 2002) indicates 6.2 wt.% MgO in the liquid on the solidus at 1 GPa and THERMOCALC (Jennings & Holland, 2015) gives 6.6 wt.%. Hence, we here recalibrate the relation for

Table 1
Parameters of the PRIMELT3-P dP Fit Equations

	dP_{LZ}						dP_{HZ}		
A_1	−0.13	B_1	1.74	X_1	−21.37	Y_1	9.079	Z_1	−0.0144
A_2	0.0101	B_2	−46.2	X_2	−72.7	Y_2	6097.2	Z_2	−5,956
A_3	120	B_3	555	X_3	1168	Y_3	−18506.4	Z_3	52,903

P_i < 2.5 GPa and liquid MgO < 12.3 wt.%, using the same *P-T*-MgO contours and the older solidus of Herzberg et al. (2000), which lacks the deep cusp, a new equation is:

$$P_i = -0.481\,\mathrm{MgO} + 0.000454\,\mathrm{MgO}^3 + 1.166\,(\ln(\mathrm{MgO}))^2 \quad (3)$$

At MgO > 12.3 wt.%, where both Equations 2 and 3 are valid, Equation 3 typically yields values of P_i that are lower by 0.20 GPa. For near-solidus experimental melt compositions on fertile peridotite KLB-1, Equation 3 gives 3.1 GPa for 15.78 wt.% MgO, which is the experimental liquid composition of Davis et al. (2011) at 3.0 GPa. Similarly, Equation 3 gives 4.9 GPa at 21.0 wt.% MgO, matching the experimental liquid of Herzberg and Zhang (1996) at 5.0 GPa. At 23.1 wt.% MgO, Equation 3 gives 6.0 GPa, the same pressure at which Tomlinson and Holland (2021) observed this liquid MgO concentration. A primary magma MgO content of 23% is a compositional upper bound on both the PRIMELT3 and PRIMELT3-P calibrations, and the algorithm does not extrapolate well. Pressures returned for primary magma solutions having MgO contents higher than ~23% are not reliable.

To obtain P_f, we need a relation between the pressure interval of melt production dP and the extent of accumulated fractional melting F_{AFM}; that is, the melt productivity (see Asimow et al., 1997). For peridotite (LZ) melting, we found that the relationship between dP and F_{AFM} in the one-dimensional forward decompression model described above could be parameterized with the empirical equation:

$$dP_{LZ} = AF_{AFM} + BF_{AFM}^2 \quad (4)$$

Readers should note that by peridotite melting we are referring to any residue other than harzburgite and dunite: this is typically lherzolite (Ol + Opx + Cpx ± Plag ± Sp ± Gt), but it may also be Opx-free (Tomlinson & Holland, 2021; Walter, 1998). There is a unique $dP_{LZ} - F_{AFM}$ melt production relationship specific to any given initial melting P_i. Results of the forward model P_i simulations at 3, 4, 5, and 7 GPa (Herzberg, 2004; Herzberg & O'Hara, 2002) produce a family of 4 curves which were fitted with the empirical equations:

$$A = A_1 + A_2 P_i^3 + A_3 P_i^{-3} \quad (5)$$

$$B = B_1 + B_2 P_i^3 + B_3 P_i^{-3} \quad (6)$$

See Table 1 for the values of the fitted parameters in Equations 5 and 6.

Melt production for harzburgite (HZ) melting is much lower than that for peridotite melting (Asimow et al., 1997), and results were modeled with the following empirical equation:

$$dP_{HZ} = X + YF_{AFM} + ZF_{AFM}^2 \quad (7)$$

where

$$X = X_1 + X_2 P_i^{-1} + X_3 P_i^{-3} \quad (8)$$

$$Y = Y_1 P_i + Y_2 P_i^{-2} + Y_3 P_i^{-3} \quad (9)$$

$$Z = Z_1 P_i^4 + Z_2 P_i^{-2} + Z_3 P_i^{-4} \quad (10)$$

See Table 1 for the values of the fitted parameters in Equations 8–10.

At the boundary between peridotite and harzburgite melting:

$$dP_{LZHZ} = 0.0831 P_i^{2} + 20.15 P_i^{-2} - 1.19 \ln(P_i), \quad (11)$$

so that:

$$dP = \begin{cases} dP_{HZ} \text{ if } dP_{LZ} > dP_{LZHZ} \\ dP_{LZ} \text{ if } dP_{LZ} \leq dP_{LZHZ} \end{cases} \quad (12)$$

And, finally, by rearrangement of Equation 1,

$$P_f = P_i - dP \quad (13)$$

Results showing the MgO and FeO contents of primary accumulated fractional melts at P_f are shown as blue curves in Figure 1.

Equations 4–13 predict the forward simulations at 3–7 GPa to within ±0.06 GPa when Equation 2 for P_i is used, but we expect the error would be much larger if applied to paths with lower P_i. Use of the preferred Equation 3 for P_i increases the uncertainty to ±0.44 GPa, but this error is dominated the decompression melting simulation with $P_i = 7$ GPa and primary magma MgO content of 23%, which is the upper bound on the PRIMELT3 calibration imposed by Walter's (1998) data. Considering the 7 GPa case as an outlier, simulations at 3, 4, and 5 GPa yield an uncertainty of ±0.23 GPa using Equation 3.

We emphasize that the method described here of computing dP as a function of F_{AFM} and P_i is entirely compositional in nature, taking no account of the energetics of melt production expected for an isentropic decompression process. The results share some features with the predictions of the thermodynamic pMELTS model (Ghiorso et al., 2002) using the isentropic calculation method of Asimow et al. (2001), but there are also a number of essential differences. In general, both models agree that melting paths that begin in the shallow part of the garnet lherzolite field (around 3 GPa), at potential temperatures near 1450°C, yield average melt productivity near 20%/GPa for lherzolite and 5%–10%/GPa for harzburgite (once clinopyroxene is exhausted). The behavior of pMELTS, however, is much more sensitive to predicted near-solidus variations in the spacing and slope of equal melt-fraction contours (see Asimow et al., 1997). Hence, pMELTS predicts that melt productivity increases along each decompression path from the solidus to a peak near $F_{AFM} \sim 0.15$, whereas PRIMELT3-P predicts monotonically decreasing melt productivity along each (anhydrous) streamline. Also, pMELTS predicts that increasing pressure (and potential temperature) leads to decreasing melt productivity due to the flattening of the solidus, whereas PRIMELT3-P predicts increasing melt productivity due to the decrease in the spacing between solidus and liquidus temperatures (Herzberg & Zhang, 1996). Although the predictions of pMELTS are thermodynamically self-consistent, it has been well-documented that they diverge from experimental constraints, especially at low melt fraction and high pressure. Asimow et al. (1997) show that thermodynamic estimates of melt productivity are dominated by the slope and spacing of equal melt fraction contours (such as the solidus), with additional contributions (especially very near the solidus) arising from correct definition of the incremental entropy of fusion. Hence these results depend primarily on the accuracy of experimental calibration of the melt fraction contours in *P-T* space, and PRIMELT3-P was developed precisely for this purpose. Although PRIMELT3-P is not a thermodynamic model of melt productivity, its results are broadly consistent with the expectations of thermodynamics if the melt fraction contours it uses are correct. Since the melt fraction contours in PRIMELT3-P are directly tied to experiments, rather than themselves being imperfect predictions of a constructed Gibbs energy model, the different productivity predictions of PRIMELT3-P and pMELTS are provocative rather than fatal for either model. Detailed reconciliation of the compositional approach of PRIMELT3-P and the thermodynamic approach to computing melt production awaits improvements in the thermodynamic model that better fit experimental constraints beyond 3 GPa.

2.3. Uncertainties

In addition to the ±0.23 GPa uncertainty arising from the forward decompression melting model, there are other layers of uncertainty that can compromise computed P_f results. Figure 1 shows that P_f isopleths can be highly

compressed in some regions of primary magma FeO-MgO space. This will most seriously impact results that yield P_f solutions between 0 and 1 GPa, which can arise from primary magma solutions that vary by just 1 wt. % MgO. Error brackets in Figure 1 also show that the 1σ uncertainty in the Fe-Mg distribution coefficient between olivine and melt, K_D, in high pressure experiments (Herzberg & O'Hara, 2002) could propagate to a range of ±1 GPa in P_f. However, it will be shown below (Section 5) that the P_f results from PRIMELT3-P have a 1σ uncertainty of about ±0.29 GPa.

2.4. PRIMELT3-P

The PRIMELT3 MEGA.xlsm Microsoft® Excel® macro-enabled workbook (Herzberg & Asimow, 2015) has been modified to include melting pressures, and is now called PRIMELT3-P MEGA.xlsm. It contains example worksheets for several specific lava compositions, which can be duplicated or re-used for single compositions, as well as the MEGA feature for batch processing of large data sets. Detailed descriptions of the software implementation and its limitations are found in Herzberg and Asimow (2015) and will not be repeated here.

PRIMELT3-P incorporates the same model of the dependence of the olivine liquidus temperature (in °C) on liquid MgO (weight percent) as previous versions:

$$T^{Ol/L}_{1\,\mathrm{bar}} = 1020 + 24.4\,\mathrm{MgO} - 0.161\,\mathrm{MgO}^2 \tag{14}$$

which was calibrated on 1249 experiments and can be applied to a wide range of melt compositions: MgO = 1 to 57 wt.%; $Na_2O + K_2O$ = 0 to 14 wt.%; SiO_2 = 30 to 70 wt.%. There is excellent agreement among olivine liquidus thermometers. Equation 14 agrees with olivine-liquid equilibrium temperatures calculated by MELTS (Ghiorso & Sack, 1995) to within ±7°C (1 σ); it is usually within 10°C of the Beattie (1993) thermometer, which is slightly more accurate (Herzberg & Asimow, 2015).

Olivine liquidus temperatures need to be corrected when they are applied at elevated pressures, including initial melting pressure (P_i), final melting pressure (P_f), and the fractionation pressure where olivine addition and subtraction are computed (P_{Frac}, a user input quantity given on each single-composition PRIMELT3-P worksheet at cell R6). This correction is expressed by

$$T^{Ol/L}(P) = T^{Ol/L}_{1\,\mathrm{bar}} + 54\,P - 2\,P^2 \tag{15}$$

which is identical to Equation 12 in Herzberg and Asimow (2015), where it was used to map the olivine saturation (liquidus) surface for primary magmas in temperature - pressure space (Herzberg & Asimow, 2015, Figures 4 and 7).

On the PRIMELT3-P single-composition worksheets, notable information appears at.

1. Cell Z15, output of initial melting pressure P_i (GPa)
2. Cell AA15, output of final melting pressure P_f (GPa)
3. Cell AB15, output of $T^{Ol/L}(P_f)$, the olivine liquidus temperature of the primary magma calculated at the final melting pressure P_f.
4. Cell P15, $T^{Ol/L}(P_{\mathrm{Frac}})$, the olivine liquidus temperature of the primary magma at the olivine fractionation pressure Frac$P$.
5. Column AE, olivine liquidus temperatures for each member of the family of liquid compositions derived by increments of 1% olivine addition to or subtraction from the input composition, computed the Beattie (1993) thermometer and corrected to Frac$P$.
6. Column AF, the Fe-Mg distribution coefficient between olivine and melt ($K_D \equiv (\mathrm{FeO/MgO})_{Ol}/(\mathrm{FeO/MgO})_{\mathrm{melt}}$) for each member of the family of liquid compositions derived by increments of 1% olivine addition to or subtraction from the input composition, computed at the temperature shown in column AE and at P_{Frac} using the Toplis (2005) model.
7. Column AG, Mg# (i.e., molar 100*MgO/(MgO + FeO) of olivine in equilibrium with each of the family of liquid compositions along the olivine control line, obtained from the melt composition and K_D.
8. Columns AE, AF, and AG are useful in simulating olivine fractionation along an olivine liquid line of descent. This is the PRIMELT "Olivine Calculator". By itself, that is, without attempting to use the full

PRIMELT3 solution outside its calibration limits, the olivine calculator can be useful for constraining primary magma compositions for komatiites that had MgO contents in excess of 23% (Herzberg, 2022).

9. Cell X15 estimates the residual mineralogy that coexisted with the computed primary magma based on its projected position in Ol-An-Qz space (see Figure 1a of Herzberg & Asimow, 2015).
10. Cell Y15 estimates the residual lithology that coexists with the computed primary magma based on its FeO-MgO contents. Residual harzburgite consists of Olivine (Ol) + Orthopyroxene (Opx) ± Spinel (Sp). Peridotite residues typically contain Ol + Opx ± Cpx ± Plag ± Sp ± Gt, but they may also be Opx- or Cpx-free at high pressures (e.g., Ol + Cpx + Gt or Ol + Opx + Gt; Walter, 1998; Jennings & Holland, 2015). The agreement between the two estimates of residual mineralogy is good, but fewer harzburgite residues are generally identified in Ol-An-Qz projection than in FeO-MgO space (Figure 1).

PRIMELT3-P may fail to find a primary magma solution in some cases. More often, however, it may find a solution but also warn the user that the solution is suspect because it fails one of the tests for validity. The solution may be compromised by pyroxenite melting, by augite fractionation/accumulation, or by volatile-rich peridotite melting. Importantly, we will show below that the identification of pyroxenite-source melts can often help to avoid erroneous pressure estimates resulting from application of models that assume a peridotite source, either PRIMELT3-P or FractionatePT3 (Lee et al., 2009), to pyroxenite-source melts.

As an alternative to the PRIMELT3-P MEGA.xlsm workbook, avoiding dependence on proprietary software and the poor support of visual basic macros on MacOS, a PRIMELT3-P python-based GUI for Windows and macOS users is provided with this paper. All primary magma calculations, compositional parameters, and pressure-temperature conditions are calculated following the same general procedure as the workbook version. There are minor and subtle differences between the python and Excel versions at the level of different interpolations between 1% olivine addition/subtraction steps. The program requires a delimited text file as input. An example input file is provided; it contains the analyzed composition of the primitive rock (in oxide weight percent), a specified FeO/FeO_T ratio, and the fractionation pressure in bars. The output is divided into two separate blocks for batch and AFM solutions, respectively, and can be exported to several formats or copied to the clipboard for pasting into any spreadsheet program. Other additional features include an FeO versus MgO plot for olivine fractionation lines and pressure-temperature estimates for each primary magma solution. Detailed instructions and input templates are available as separate text files included in the package. Both the excel and GUI version of PRIMELT3-P can be downloaded for free from Gitlab (https://gitlab.com/primelt_software/primelt3-p) and from a Caltech data repository https://doi.org/10.22002/6te59-vad07.

2.5. Oxidation State of Iron

The oxidation state of iron in a primitive magma must be known or assumed because the primary magma solution depends on FeO content (Figure 1), not Fe_2O_3 content. It is therefore necessary to calculate FeO from total iron FeO_T, and this is done by inputting FeO/FeO_T in Cell F5 in a single-composition PRIMELT3-P worksheet or in the input tables to the MEGA function or the python GUI. The consequences of changing the assumed FeO/FeO_T in primary magma estimates have been explored by Asimow (2022).

There is now a significant literature on the oxidation state of iron in MORB and OIB constrained from wet chemistry, Mössbauer spectroscopy, and X-Ray absorption near-edge structure (XANES) spectroscopy on volcanic glasses and melt inclusions (Berry et al., 2018; Bézos et al., 2021; Cottrell et al., 2022; Gaborieau et al., 2020). However, all measurements have been made on compositions that are substantially different from the primary magmas of interest owing to magma chamber recharge, mixing, tapping, assimilation and crystallization (Coogan & O'Hara, 2015; O'Hara & Herzberg, 2002; O'Neill & Jenner, 2016). Additionally, degassing can reduce iron (e.g., Brounce et al., 2017; Hartley et al., 2017; Moussallam et al., 2016).

But even if we can reconstruct a primary magma FeO content from a lava with an accurate measurement of its FeO/FeO_T on eruption and by properly evaluating its crystallization and degassing history, there is added ambiguity about whether the FeO/FeO_T at the liquidus at P_{Frac} accurately represents redox conditions of the mantle during melting. Jennings and Holland (2015) estimate that the fO_2 of a fertile peridotite source at pressures and temperatures relevant to primary magmas in this study can be lower by 1–2 log units relative to the crust where crystallization and degassing typically take place. This implies that primary magmas may become oxidized on their way to the surface. One log unit of oxidation may decrease the FeO/FeO_T from, for example, 0.90 in the mantle

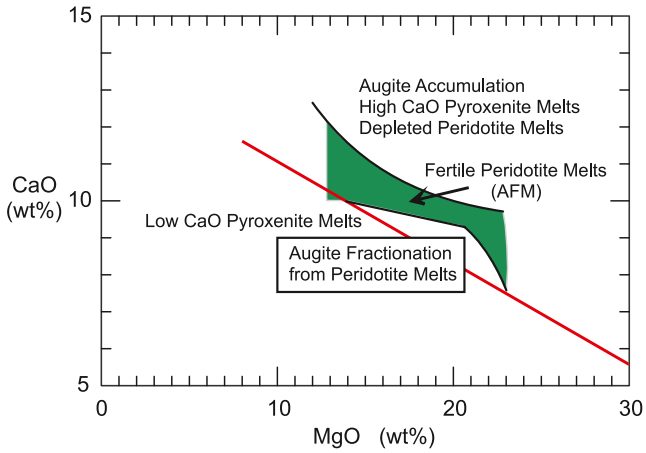

Figure 2. CaO contents of primary melts of fertile peridotite KR-4003 formed by accumulated fractional melting (AFM; green space), modified after Herzberg and Asimow (2008). Primary melt compositions having CaO contents higher and lower can have multiple origins as discussed in the text; for these, pressures obtained from PRIMELT3-P will be erroneous.

to 0.86 in the crust (calculated using rhyoliteMELTS; Gualda et al., 2012). Decompression melting from larger values of P_f at ocean islands compared to mid-ocean ridges may therefore contribute, at least in part, to the apparently more oxidized nature of mantle plume magmas compared with MORB (Bézos et al., 2021; Brounce et al., 2017; Gaborieau et al., 2020; Hartley et al., 2017; Moussallam et al., 2016, 2019). On the other hand, the sources of plumes magmas may already be oxidized by incorporation of recycled crust or delaminated lithospheric mantle (Brounce et al., 2017; Helz et al., 2017; Moussallam et al., 2016, 2019; Shorttle et al., 2015).

The default assumption made in PRIMELT3-P is that melts have $FeO/FeO_T = 0.90$, consistent with most measurements on MORB glasses (Berry et al., 2018; Bézos et al., 2021; Gaborieau et al., 2020), noting that other groups estimate $FeO/FeO_T = 0.86$ for MORB (Cottrell et al., 2022). However, we will consider below the possibility of more oxidized conditions in plume-derived lavas. The effect of decreasing FeO/FeO_T is to lower the estimate of final melting pressure P_f.

2.6. Source Lithology

The source lithology of a primary magma must be known because the PRIMELT3-P parameterization has been calibrated from experiments on fertile peridotite KR-4003 and because olivine-liquid equilibrium in the source is assumed in constructing the FeO-MgO relations. Therefore, pressure estimates and primary magma solutions from PRIMELT3-P for a rock that was generated from a pyroxenite source will be erroneous. The FractionatePT3 algorithm of Lee et al. (2009), which assumes that primary melts were in equilibrium with Ol + Opx, likewise will fail when applied to pyroxenite-derived melts, many of which may have Cpx + Gt ± Ol residues (Herzberg, 2011; Kogiso et al., 1998, 2004; Lambart et al., 2016).

How, then, might we confidently identify and filter pyroxenite-source lavas? The use of trace element and radiogenic isotopic compositions of basalts to identify source lithology is fraught with difficulties. These tracers can reveal the influence of recycled crust in the source, but generally do not distinguish whether the recycled crust was present as discrete masses of pyroxenite or only as enriched peridotite (e.g., Herzberg, 2011). The identification of source lithology in PRIMELT3 is made tractable because there is a narrow range of CaO contents of both experimental and model accumulated fractional melts of peridotite KR-4003 as shown in Figure 2. This leads to the filter that separates low-CaO pyroxenite-source melts from the CaO contents of melts of fertile peridotite by dividing at the red line in Figure 2 given by Equation 7 in Herzberg and Asimow (2008),

$$\mathrm{CaO} = 13.81 - 0.274\,\mathrm{MgO} \quad (16)$$

where CaO and MgO are expressed in weight percent. We assume that this CaO-MgO filter is useful even for refertilized peridotite. But it is imperfect—it does not always exclude melts that are in fact sourced from pyroxenite. For example, in a database of 91 melt compositions having MgO >10% obtained from melting experiments on pyroxenites (Lambart et al., 2013, 2016), Equation 16 successfully identifies 76% of the pyroxenite melt compositions as low-CaO pyroxenite-source melts that cannot be derived by melting of fertile peridotite KR-4003. Unfortunately, the remaining 24% of the pyroxenite-source melts are above the line of Equation 16 and are not flagged as impossible peridotite-source melts. Indeed, some partial melts of peridotite and pyroxenite can have similar compositions, as demonstrated previously (Lambart et al., 2009), and so PRIMELT3 cannot always distinguish them.

As discussed below, most high MgO shield-stage lavas from Hawai'i are natural examples of low-CaO pyroxenite-source melts, falling below the line of Equation 16 and so outside the range of partial melts of peridotites KR-4003 (Davis et al., 2011; Herzberg, 2006, 2011; Herzberg & Asimow, 2008). Calculations with recent multicomponent melting models incorporated into THERMOCALC concur that melts of peridotite sources KLB-1 (Jennings & Holland, 2015) and KR-4003 (Tomlinson & Holland, 2021) never have CaO (at equal MgO) as low as these Hawai'ian shield-stage lavas. Primary magmas on the solidus with 15%–21% MgO were modeled

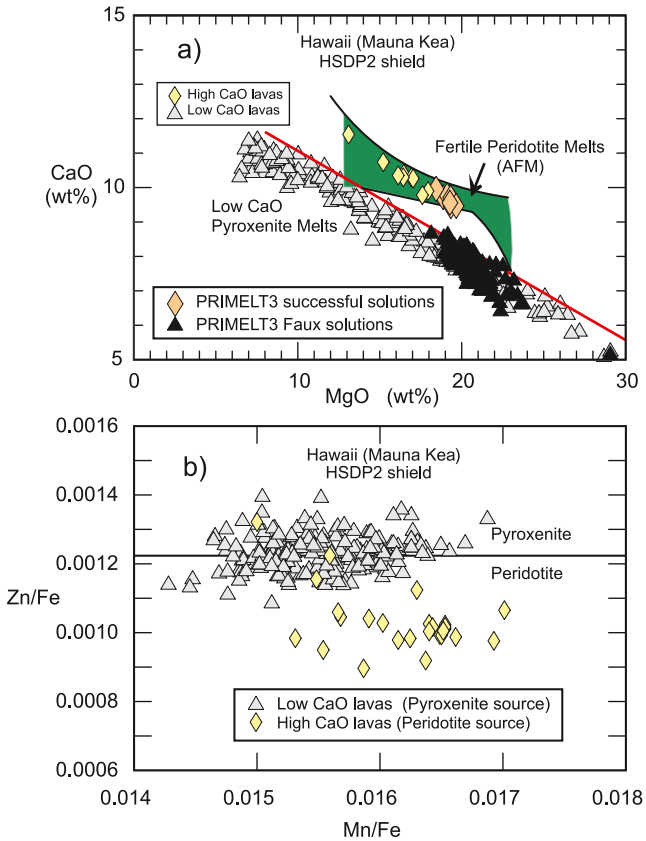

Figure 3. (a) CaO and MgO contents of high- and low-CaO shield-stage lavas from Mauna Kea and their successful and unsuccessful PRIMELT3 primary melts, respectively, using $FeO/FeO_T = 0.90$. Unsuccessful solutions for the low-CaO lavas are called "Faux solutions" because the primary magma compositions and pressures obtained were calculated from a peridotite-source melting calibration, not appropriate for pyroxenite-source melting. Lavas with intermediate CaO contents yield PRIMELT3 "augite fraction" error flags and are not shown for clarity. (b) Zn/Fe for high- and low-CaO shield-stage lavas from Mauna Kea as a proxy for source lithology (Le Roux et al., 2011).

to have 10% CaO (Herzberg & Asimow, 2008), similar to model results of Tomlinson and Holland (2021). It is therefore no surprise that olivines that crystallize from Hawai'ian shield-stage lavas have CaO contents that are also lower than olivines that crystallize from melts of a peridotite source provenance (Gavrilenko et al., 2016; Sobolev et al., 2007).

Primary magmas can have CaO contents that are too high to be accumulated fractional partial melts of peridotite KR-4003. For these, PRIMELT3 identifies them as resulting from "augite accumulation" if they have CaO contents higher than those defined by equation 9 in Herzberg and Asimow (2008):

$$CaO = 1.095 + 0.154\,MgO + 116.58\,MgO^{-1} \quad (17)$$

However, we recognize that these high-CaO primary magma solutions can have origins other than augite accumulation. First, of the 91 experimental pyroxenite melts (Lambart et al., 2013, 2016), 20% are above the curve defined by Equation 17 and PRIMELT3-P erroneously flags them as having experienced "augite accumulation". Therefore, Equation 17 is also potentially useful for identifying high-CaO pyroxenite source melts. Second, Shorttle and Maclennan (2011) and Shorttle et al. (2014) reported a wide range of CaO contents for primitive Icelandic lavas and found that CaO in these lavas is negatively correlated with Nb/Zr and $^{87}Sr/^{86}Sr$. As discussed below, application of PRIMELT3-P to this Icelandic database yields many successful solutions with no errors. However, the samples with the highest CaO contents are flagged for "augite accumulation". In fact, it is likely that these lavas have high CaO instead because they were derived from a strongly depleted peridotite source composition (Shorttle & Maclennan, 2011; Shorttle et al., 2014); this is discussed below in Section 4.6.

Another critical application of the CaO filters is identification of peridotite-source melts that have fractionated augite, which leads to rapidly increasing FeO_T and erroneous primary magma solutions with excessive potential temperature estimates. These low-CaO fractionated melts may plot below the line of Equation 16 and be flagged as "pyroxenite source … no solution". So, the user will know to exclude these lavas, but for the wrong reason. By contrast, lavas that plot in the narrow region of CaO-MgO space below peridotite-source melts and above low-CaO pyroxenite-source melts are specifically flagged with an "augite fractionation" warning.

3. Mauna Kea, Hawai'i

3.1. Background

We begin by examining magmatic pressure estimates for Hawai'i using both PRIMELT3-P and FractionatePT3 (Lee et al., 2009). Hawai'i is an ideal test case for petrological pressure estimates because it is an iconic mantle plume that impacts an older part of the Pacific lithospheric plate, whose local thickness has been independently constrained from seismology to be 75–93 km (Rychert et al., 2013; Schmerr, 2012).

Most lava samples from the major shield-stage volcanoes of the Hawai'ian chain trigger the error flag for low-CaO pyroxenite melts. The inference is that pyroxenite is a major source lithology in the Hawai'ian plume (Herzberg, 2006, 2011; Sobolev et al., 2007). By contrast, the post-shield lavas from Mauna Kea stand out, among Hawai'ian samples, in providing successful PRIMELT3 primary magma solutions for peridotite source melting; mantle potential temperature estimates for these samples are discussed in Herzberg and Asimow (2008). Here, we focus on the shield-stage lavas from Mauna Kea obtained from the Hawai'i Scientific Drilling Project 2 (HSDP2), which erupted from 695,000 to 209,000 years ago (Rhodes et al., 2012; Stolper et al., 2004, 2009). Most samples of the core analyzed and reported by Rhodes and Vollinger (2004) have CaO contents that are lower than those defined by Equation 16, consistent with pyroxenite source melting (Figure 3a). For these low-CaO

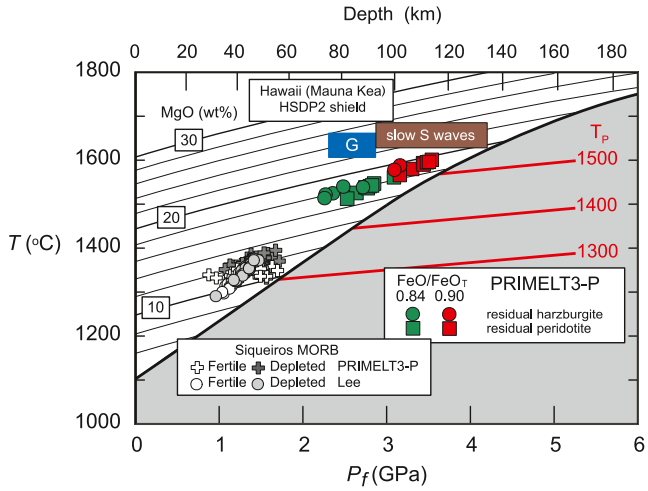

Figure 4. PRIMELT3-P final melting pressures P_f and temperatures of primary magmas for high-CaO shield-stage lavas from Mauna Kea obtained from the Hawai'i Scientific Drilling Project 2 (HSDP2) (DeFelice et al., 2019) at different assumed oxidation states of iron. "G" refers to the Gutenberg Discontinuity, or LAB, for the Pacific oceanic lithospheric plate at the location of Hawai'i (75–93 km; Schmerr, 2012; Rychert et al., 2013). Slow S waves are melt distributions that have been mapped below Hawai'i using receiver functions (Rychert et al., 2013). Siqueiros MORB solutions: $FeO/FeO_T = 0.90$; fertile source is KR-4003 with 38.1% MgO and 8.0% FeO; depleted source has 38.1% MgO and 7.7% FeO and primary magmas crystallize olivine phenocrysts with Mg# = 91.0 ± 0.1.

lavas, PRIMELT3 calculates a primary magma solution, but it flags the result with a "pyroxenite source" warning. We label these apparent results as "faux" solutions because the primary magma compositions and pressures obtained were calculated from a peridotite-source melting calibration, not appropriate for pyroxenite-source melting.

Rare lavas with high CaO contents occur in the HSDP core in the depth intervals 1766–1782 and 1795–1808 m below sea level. Whole rock data reported by DeFelice et al. (2019) and their PRIMELT3 primary magma solutions are provided in Table S1. These primary magmas plot in the green space of solutions in Figure 3a, consistent with a peridotite source lithology. The lavas are distinguished from all other shield-stage lavas from Mauna Kea in having depleted Nd, Hf, and Sr isotope ratios (DeFelice et al., 2019). These authors proposed a mantle plume structure having enriched components embedded within a refractory depleted matrix. While DeFelice et al. (2019) did not specify the lithological nature of these components, their model is consistent with pyroxenite bodies contained within a peridotite matrix (Herzberg, 2006, 2011), yielding low- and high-CaO lavas descended from primary magmas generated in pyroxenite and peridotite lithologies, respectively (Figure 3a).

The fidelity of CaO as a probe of lithological heterogeneity in the source is supported by Zn/Fe data from Mauna Kea shield-stage lavas, as shown in Figure 3b (DeFelice et al., 2019; Huang & Humayun, 2016; Rhodes & Vollinger, 2004). Zn and Fe are strongly fractionated by Cpx and Gt but negligibly so by Ol and Opx (Le Roux et al., 2011). Hence, pyroxenite-source melts and olivines crystallized from them can have higher Zn/Fe than those from peridotite (Howarth & Harris, 2017; Le Roux et al., 2011). The generally higher Zn/Fe in low-CaO Mauna Kea lavas is therefore consistent with pyroxenite source melting as inferred from Equation 16. Some low-CaO lavas interpreted here as pyroxenite-source fall into the peridotite field, defined by Le Roux et al. (2011) as Zn/Fe < 0.0012. However, it is not likely that there is a completely clean demarcation between the two lithologies. At the contact between a body of olivine-absent pyroxenite (Cpx + Gt ± Qz/Cs) and its olivine-dominated peridotite host, there may be a reaction zone consisting of olivine pyroxenite (Ol + Cpx + Gt; see Figure 16 in Herzberg, 2011). Melts at these contact zones are expected to have variable Zn/Fe, depending on the amount of residual olivine. Likewise, some high-CaO lavas have Zn/Fe in or near the pyroxenite field, possibly owing to refertilization of peridotite by pyroxenite-source melts. These complexities notwithstanding, it is clear from Figures 3a and 3b that there is a separation of Zn/Fe between the high and low-CaO Mauna Kea populations, consistent with lithological variability. The consequences of such source variability for magmatic pressure estimates are discussed below in Section 3.4.

3.2. Oxidation State of Iron and Seismological Constraints

Results of P_f and $T^{Ol/L}(P_f)$ for the high-CaO Mauna Kea lavas interpreted as peridotite-source (DeFelice et al., 2019) are shown in Figure 4, calculated with $FeO/FeO_T = 0.84$ and 0.90. The more oxidized condition was suggested by Brounce et al. (2017) based on XANES observations of HSDP2 low-CaO lavas having ~7% MgO, corrected to their preferred primary magma with 19% MgO. It is unclear whether this oxidation state should be applied to the high-CaO samples from the same core. The following are noteworthy observations:

1. Computed values of P_f for the reduced model range from 3.1 to 3.5 GPa. The effect of assuming a more oxidized condition is to reduce P_f by a depth equivalent of about 25 km. Mantle potential temperature (T_P) solutions are 1520–1560°C for the reduced models and uniformly 30°C lower for the oxidized assumption. These results are similar to those for post-shield lavas from Mauna Kea (Herzberg & Asimow, 2008). The calculations for a particular example, Mauna Kea HSDP2 sample SR0684–8.95 (Stolper et al., 2004) with $FeO/FeO_T = 0.90$, is included in the PRIMELT3-P MEGA.xlsm file; for this sample, T_P is 1526°C.
2. For $FeO/FeO_T = 0.90$, there is substantial agreement between the estimates of melting pressure from PRIMELT3-P and inferences of melt distribution in the mantle below Hawai'i using receiver functions

(Rychert et al., 2013). The range of P_f for the high-CaO HSDP2 suite is equivalent to depths of final melting of 100–115 km, identical to the depths showing greatest S wave velocity reduction (Rychert et al., 2013). This result is promising, but we caution that the Hawai'ian mantle plume structure inferred from present-day seismological work may differ from that during Mauna Kea shield-building time (695–209 ka).

3. For $FeO/FeO_T = 0.90$, P_f results are higher than those defined by the Gutenberg Discontinuity, inferred to represent the lithosphere-asthenosphere boundary (LAB), mapped beneath Hawai'i at 75–93 km depth (Rychert et al., 2013; Schmerr, 2012). This result is consistent with models suggesting that the LAB is a barrier to vertical mantle plume transport and melting (e.g., Niu et al., 2011; Prytulak & Elliott, 2007).
4. The P_f results from PRIMELT3-P are lower than the seismological LAB when assuming $FeO/FeO_T = 0.84$. We interpret this result to imply that the low-CaO pyroxenite-source lavas on which the XANES measurements were made (Brounce et al., 2017) are more oxidized than the high-CaO peridotite-source lavas owing to crust recycling. Alternatively, there may have been oxidation at some stage between melting and sampling (see Section 2.5).

3.3. Hawai'i Compared to Ambient Mantle

Results for Hawai'i are compared with the ambient mantle reference frame as represented by 35 primitive Ol-phyric mid-ocean ridge basalt samples from the Siqueiros Fracture Zone (Arevalo & McDonough, 2010; Hays, 2004; Herzberg & Asimow, 2015; Perfit et al., 1996). Predicted maximum olivine Mg# in liquidus olivine for this suite is 90.4 when calculated assuming the default PRIMELT3 source composition (KR-4003 with 38.1% MgO and 8.0% FeO). However, observed olivine phenocrysts in these samples extend up to Mg# 91.0 (Coogan et al., 2014; Sobolev et al., 2007). We can resolve this difference by reducing the FeO content of the peridotite source composition in Cell R3 of the PRIMELT3 worksheet from 8.0% to 7.6%. This FeO-depleted peridotite source yields more primitive primary magma solutions, with Mg# of 91.0 for liquidus olivine and correspondingly higher MgO in the primary liquid (by about 1 wt.%). Although the more depleted source assumption also increases estimated T_P from 1340 ± 10°C to 1365 ± 14°C, there is no change in the mean estimate of final pressure of melting, $P_f = 1.4$ GPa (Figure 4). We do not know precisely how robust the calibration of P_f is to variations in peridotite source FeO content; Supporting Information S1 provides a deeper analysis of the effects of peridotite source composition on PRIMELT3 solutions.

Many models of the MORB source composition have about 8.0% FeO (Lyubetskaya & Korenaga, 2007; McDonough & Sun, 1995; Palme & O'Neill, 2003), including the depleted MORB mantle DMM of Workman and Hart (2005). Hence it is worth considering whether there are alternatives to supposing that the Siqueiros suite is derived from a source with 7.6% FeO. (a) This may in fact be a low-FeO domain that arose from extraction of ancient, high-temperature FeO-rich melts (Text S1 in Supporting Information S1; Herzberg et al., 2010; Herzberg & Rudnick, 2012). Alternatively, (b) the Siqueiros primary magma may have formed by imperfect mixing of extracted melt increments, with biased oversampling of high-F fractional melts from the upper parts of the melting region (progressive decompression melting always yields decreasing FeO in the residues; Herzberg & O'Hara, 2002).

Our preferred mantle potential temperature for Siqueiros, 1365 ± 14°C, is about 200°C lower than Hawai'i (Figure 4). Other recent petrological T_P estimates for Siqueiros MORB are 1364 ± 23°C (Matthews et al., 2021) and 1318 + 44/−32°C (Matthews et al., 2016). For Siqueiros sample D-20-15, we obtain $T_P = 1357$°C with 8.0% FeO in the peridotite source or 1384°C assuming 7.6% FeO in the source (see the example worksheet "Siqueiros MORB" in the PRIMELT3-P MEGA.xlsm). By contrast, the inversion method of Krein et al. (2021), yields 1270°C for sample D-20-15.

Now, let us compare the PRIMELT3-P final pressure result for Siqueiros MORB with the pressure estimate from FractionatePT3 (Lee et al., 2009). Since the FractionatePT3 barometer was calibrated from experiments, it implicitly assumes equilibrium melting, whereas we are reporting accumulated fractional melting results for PRIMELT3-P. The FractionatePT3 software provides an option to compute T and P of an input without correcting for olivine addition or subtraction. This is useful for the present purpose because the primary magma solution from PRIMELT3-P can be tested directly, facilitating a direct comparison of calculated conditions from the two models at equal composition. Mean P_f values are 1.4 and 1.3 GPa for PRIMELT3-P and FractionatePT3, respectively. As demonstrated below, similar pressures are also obtained from both methods when applied to Hawai'i and Iceland.

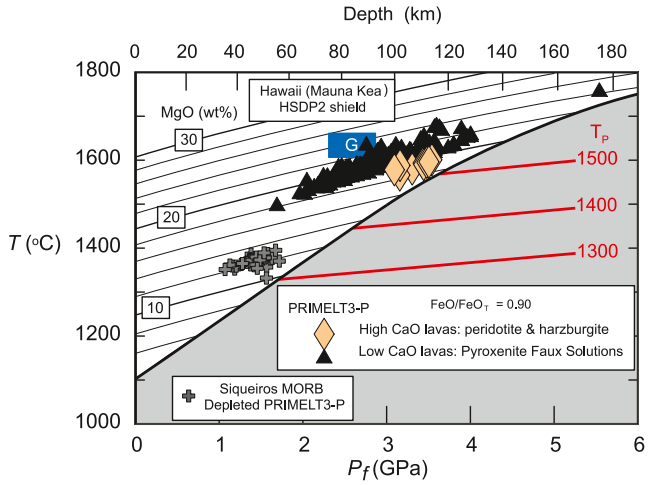

Figure 5. The effect of source lithology on computed pressures of melting. PRIMELT3-P final melting pressures P_f and temperatures of primary magmas for both high-CaO lavas (DeFelice et al., 2019) and low-CaO shield-stage lavas (Rhodes & Vollinger, 2004) from Mauna Kea obtained from the Hawai'i Scientific Drilling Project 2 (HSDP2). See Figure 3 for Zn to Fe ratios. Low-CaO lavas are identified as pyroxenite source, and pressures are called "faux" pressures because they were calibrated for peridotite source melting, not pyroxenite melting. They show the error stemming from the inappropriate application of PRIMELT3 to melts that formed from a pyroxenite source. "G" refers to the Gutenberg Discontinuity (75–93 km; Schmerr, 2012; Rychert et al., 2013).

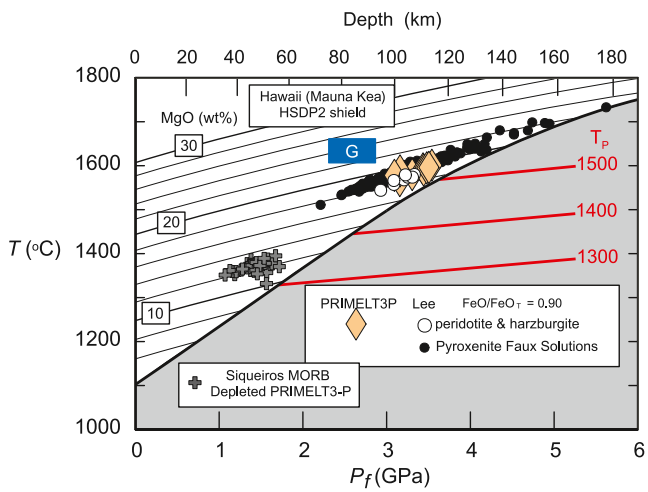

Figure 6. PRIMELT3-P and FractionatePT3 Lee et al. (2009) results for primary magmas of both high-CaO lavas (DeFelice et al., 2019) and low-CaO shield-stage lavas (Rhodes & Vollinger, 2004) from Mauna Kea obtained from the Hawai'i Scientific Drilling Project 2 (HSDP2). See Figure 3 for Zn to Fe ratios. Both methods yield similar pressures for high-CaO primary magmas extracted from lherzolite and harzburgite residues. Faux pressures obtained on the low-CaO lavas are identified by PRIMELT3-P as pyroxenite source. "G" refers to the Gutenberg Discontinuity (75–93 km; Schmerr, 2012; Rychert et al., 2013).

3.4. Compromising Effects of Pyroxenite Melting

As discussed in Methods Section 2.6, PRIMELT3-P pressure information obtained from a primary magma that was generated from a pyroxenite source will be erroneous. PRIMELT3-P identifies the low-CaO lavas (Rhodes & Vollinger, 2004) with a pyroxenite source using Equation 16, consistent with their high Zn/Fe ratios (Figure 3). It calculates faux primary magmas and their pressures anyway, and results are shown in Figure 5. This exercise is useful for evaluating the errors that result from the inappropriate application of a peridotite geobarometer to pyroxenite melts. Erroneous faux pressures range from ~2 to 6 GPa, in contrast with 3.1–3.5 GPa for successful PRIMELT3-P solutions with residual peridotite and harzburgite. Inferred mantle potential temperatures T_P obtained from the highest faux pressures can be ~100°C too high (Figure 5). Erroneous interpretations stemming from faux pressures highlight the need to distinguish melts from peridotite and pyroxenite sources.

3.5. PRIMELT3-P and FractionatePT3 Lee et al. (2009) on Mauna Kea Shield Lavas

Results shown in Figure 6 demonstrate that PRIMELT3-P and FractionatePT3 (Lee et al., 2009) yield very similar pressures for the high-CaO Mauna Kea lavas that we judge to have been extracted from peridotite and harzburgite residues: mean pressures are 2.9–3.3 GPa from FractionatePT3 and P_f is 3.1–3.5 GPa from PRIMELT3-P. Pressures/depths from both methods are slightly higher than those defined by the Gutenberg Discontinuity, or LAB, for the Pacific oceanic lithospheric plate at the location of Hawai'i, as would be expected if it were a barrier (Figure 6). Faux solutions provided by FractionatePT3 for the low-CaO primary melts yield a wide range of pressures, from 2 to 6 GPa. For these faux solutions, there is no guarantee that such pyroxenite source melts were extracted from a residue containing Ol + Opx, a requirement of the FractionatePT3 calibration. We do not know the nature of the residual mineralogy, but similar low-CaO lavas are found in Iceland (Shorttle & Maclennan, 2011); these authors matched them with partial melts of pyroxenite KG2 (Kogiso et al., 1998) having residual Ol + Cpx + Gt.

FractionatePT3 was also run on the same 91 experimental pyroxenite-source melt compositions (Lambart et al., 2013, 2016) discussed in Section 2.6, with the constraint of adding/subtracting olivine to a targeted Fo_{90} composition using K_D = 0.30. Unlike PRIMELT3, FractionatePT3 does not flag magma compositions that are outside of its calibration bounds. Only 10% of the experimental pyroxenite melts were in equilibrium with Ol + Opx as required by the FractionatePT3 calibration (Lee et al., 2009), but the code reports apparent primary magma compositions, temperatures and pressures for the remaining 90% of the experimental database, even though they are not in equilibrium with Ol + Opx.

These tests on experimental melts of pyroxenite reveal that neither PRIMELT3-P nor FractionatePT3 are equipped to provide meaningful temperatures and pressures of melting in all cases. However, unlike FractionatePT3, PRIMELT3-P does provide a means for identifying compromised solutions, albeit in an imperfect way as discussed in Section 2.6. Reference to Figure 6 shows that the use of FractionatePT3 on pyroxenite-source magmas from Mauna Kea can yield absolute temperatures and pressures that are both too low and too high. As with PRIMELT3-P, the mantle potential temperatures inferred from the highest faux pressures are ~100°C too high (Figure 6).

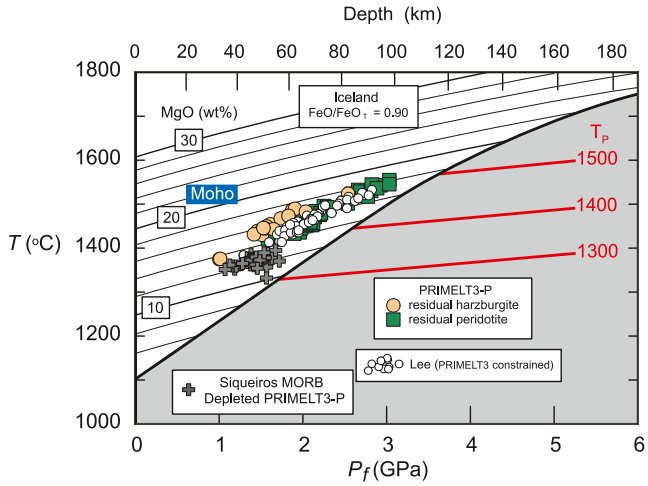

Figure 7. Pressures and temperatures of successful primary magma solutions for basalts from Iceland with FeO/FeO$_T$ = 0.90 from PRIMELT3-P. "Lee (PRIMELT3-P constrained)" refers to the implementation of FractionatePT3 (Lee et al., 2009) on those successful PRIMELT3-P primary magma compositions that are compatible with the calibration on fertile peridotite KR-4003.

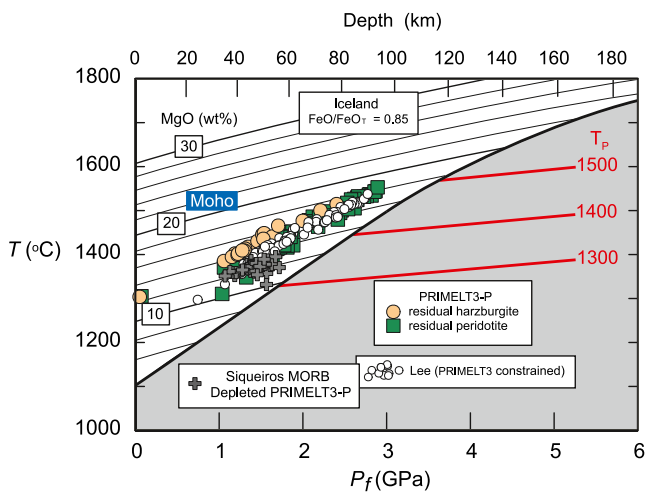

Figure 8. Pressures and temperatures of successful primary magma solutions for basalts from Iceland with FeO/FeO$_T$ = 0.85 from PRIMELT3-P. "Lee (PRIMELT3-P constrained)" refers to the implementation of FractionatePT3 (Lee et al., 2009) on those successful PRIMELT3-P primary magma compositions that are compatible with the calibration on fertile peridotite KR-4003.

4. Iceland

4.1. Background

Next, we examine magmatic pressure estimates for Iceland using both PRIMELT3-P and FractionatePT3. Iceland is an ideal complementary test case for comparison to Hawai'i because many primitive olivine-saturated lavas are available and yet its ridge-centered setting suggests much thinner lithosphere and hence lower magmatic pressures than in Hawai'i. A reasonable null hypothesis for the melting regime underneath Iceland is that melting stops at the base of the 20–40 km thick crust (Jenkins et al., 2018; Maclennan et al., 2001; Matthews et al., 2016; Shorttle et al., 2014).

We use the Iceland geochemical database featured in Shorttle et al. (2014), who used the data to model the consequences of lithological variability for mantle plume buoyancy and estimates of mantle potential temperature. Basalts and their successful PRIMELT3-P solutions are archived in Table S2. We noted above (Section 2.6) that CaO contents of primitive lavas can be used to constrain (imperfectly) source lithology; the Icelandic database features a wide range of CaO contents and negative correlations between CaO (at constant MgO) and both Nb/Zr and $^{87}Sr/^{86}Sr$ (Shorttle et al., 2014).

4.2. Oxidation State of Iron and Seismological Constraints

As with Hawai'i, we begin by examining assumptions about the oxidation state of iron and how it impacts pressure estimates. Results are shown in Figures 7–9 for FeO/FeO$_T$ = 0.90, 0.85, and 0.82, respectively. The most oxidized condition is based on XANES measurements on olivine-hosted melt inclusions and glasses from the 1783 CE Laki eruption (Hartley et al., 2017). It is slightly more oxidized than samples from the Reykjanes Ridge closest to Iceland (0.85; Shorttle et al., 2015). As with Hawai'i, we again wish to compare estimates of temperature and pressure conditions in the melting regime between the PRIMELT3-P and FractionatePT3 (Lee et al., 2009) models and so, to avoid confounding the different methods of inverting for melting conditions with the different methods of estimating primary magma compositions, we again apply FractionatePT3 to successful PRIMELT3-P primary magma compositions (shown as "Lee (PRIMELT3-P constrained)" in the figures) rather than directly to sampled compositions. We only show primary magma solutions that are compatible with the calibration on fertile peridotite KR-4003, not the faux P_f solutions obtained from pyroxenite source melts. We find the following:

1. As with Hawai'i, there is substantial agreement in magmatic pressures obtained from PRIMELT3-P and FractionatePT3.
2. For all choices of oxidation states of iron, both models yield a significant range of magmatic pressures among the Iceland samples, a result that will be addressed below.
3. For FeO/FeO$_T$ = 0.90 (Figure 7), with the exception of one low-pressure outlier, both methods yield a minimum pressure corresponding to a depth of 45–50 km. This minimum depth is slightly higher than the maximum measured depth to the seismic Moho, 44 km (Jenkins et al., 2018).
4. For FeO/FeO$_T$ = 0.85 (Figure 8), minimum pressures from both methods are lower, about 35 km, which is still well within the range of seismic Moho depths observed at different places beneath Iceland, 20–44 km. Hence the modeling results are consistent with, though they may not require, a moderately oxidized Icelandic mantle plume (Shorttle et al., 2015) or some oxidation between source and sample collection (Section 2.5).

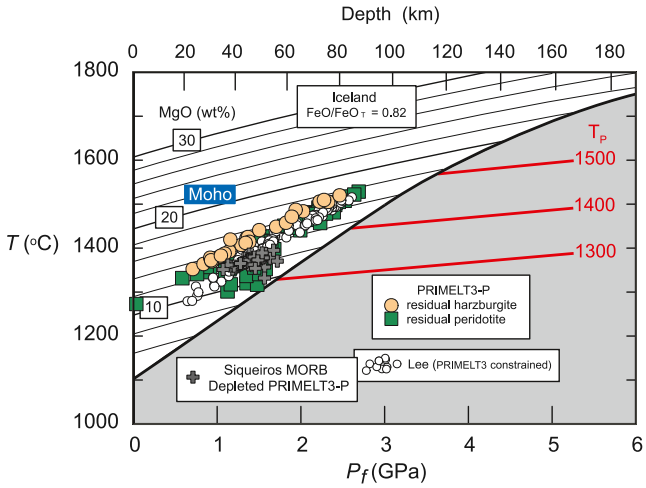

Figure 9. Pressures and temperatures of successful primary magma solutions for basalts from Iceland with FeO/FeO$_T$ = 0.82 from PRIMELT3-P. "Lee (PRIMELT3-P constrained)" refers to the implementation of FractionatePT3 (Lee et al., 2009) on those successful PRIMELT3P primary magma compositions that are compatible with the calibration on fertile peridotite KR-4003.

5. For FeO/FeO$_T$ = 0.82 (Figure 9), both methods yield minimum pressures/depths that are lower than the depth to the seismological Moho under any part of Iceland.

4.3. Mantle Potential Temperature (T_P) for Iceland

1. Mantle potential temperature estimates for the Iceland suite are quite similar between the fractional PRIMELT3 model and the batch FractionatePT3 model. For each choice of oxidation state considered, the suite of Iceland compositions yields a range of mantle potential temperatures. The significance of this heterogeneity in primary magmas will be discussed in the following section.
2. For FeO/FeO$_T$ = 0.85 and 0.90 (Figures 7 and 8) both methods agree that the maximum T_P below Iceland is 1520°C. For FeO/FeO$_T$ = 0.85 (Figure 8), the minimum T_P extends down to ~1340°C, similar to ambient mantle as represented by Siqueiros MORB.
3. Results for T_P maxima in this work (1470–1520°C) are in good agreement with previous studies: 1480–1520°C (Maclennan et al., 2001), 1428–1523°C (Brown & Lesher, 2014), 1455–1480°C (Brown et al., 2020), >1460°C (Shorttle et al., 2014), 1480°C (Matthews et al., 2016), 1525°C (Matthews et al., 2021), and 1440–1515°C (Herzberg & Asimow, 2015; Herzberg et al., 2007; Herzberg & Gazel, 2009).
4. The maximum T_P of 1520°C obtained in this study is from samples in the Western Volcanic Zone. Higher mantle potential temperatures might exist in south/central Iceland where the mantle plume center has been postulated to occur (Breddam et al., 2000; Harðardóttir et al., 2018; Maclennan et al., 2001) and where we have no samples to work with.

4.4. An Independent Test for Thermal Heterogeneity in the Icelandic Mantle Plume

Mantle potential temperature can be related to olivine liquidus temperature at 1 atm Herzberg and Asimow (2015) fit this relationship with

$$T_P = 1.049\,T^{Ol/L}_{1\,\mathrm{bar}} - 0.00019\left(T^{Ol/L}_{1\,\mathrm{bar}}\right)^2 + 1.487\cdot 10^{-7}\left(T^{Ol/L}_{1\,\mathrm{bar}}\right)^3 \quad (18)$$

Therefore, the range of T_P values for the Iceland suite, 1340–1520°C, should correlate with a range in calculated olivine liquidus temperatures (as well as a range in liquidus olivine Mg# values). For each primary magma solution, the PRIMELT3-P spreadsheet gives $T^{Ol/L}_{1\,\mathrm{bar}}$ according to Beattie (1993) in cell O15 and according to Herzberg and Asimow (2015) in cell P15, as well as liquidus olivine Mg# in cell S15. We repeated these calculations with source peridotite compositions with 8.0% and 7.3% FeO (see in Supporting Information S1). As an independent test, these PRIMELT3 solutions for olivine composition and crystallization temperatures are compared (Figure 10a) with olivine Mg# and Al-in-Ol temperatures reported by Spice et al. (2016) and Matthews et al. (2016), using the experimental calibration of Coogan et al. (2014). Assuming 8.0% FeO in the source, PRIMELT3 olivine liquidus temperatures for Icelandic primary magmas range from 1280 to 1410°C and their first crystallizing olivines have Mg# from 90.3 to 91.8, in good agreement with the high end of the observed olivine temperatures and compositions. However, several factors can complicate these comparisons.

Continuous magmatic evolution below the liquidus is expected to generate a series of olivine crystals with both Al-in-Ol temperature and Mg# decreasing below their maximum (liquidus) values. Two examples are shown in Figure 10a as black curves, obtained using the "Olivine Calculator" in PRIMELT3 (Section 2.4); each curve is a "Crystal Line of Descent", or CLD, a term coined by Putirka et al. (2011). Many, but not all, Al-in-Ol solutions overlap the two CLD possibilities, but there is a population at lower Mg# or higher temperature than the upper CLD. Elevated Al-in-Ol temperatures for low Mg# olivines can arise from diffusive resetting, given the slow diffusivity of Al compared to Fe-Mg interdiffusion in olivine (Coogan et al., 2014; Matthews et al., 2021;

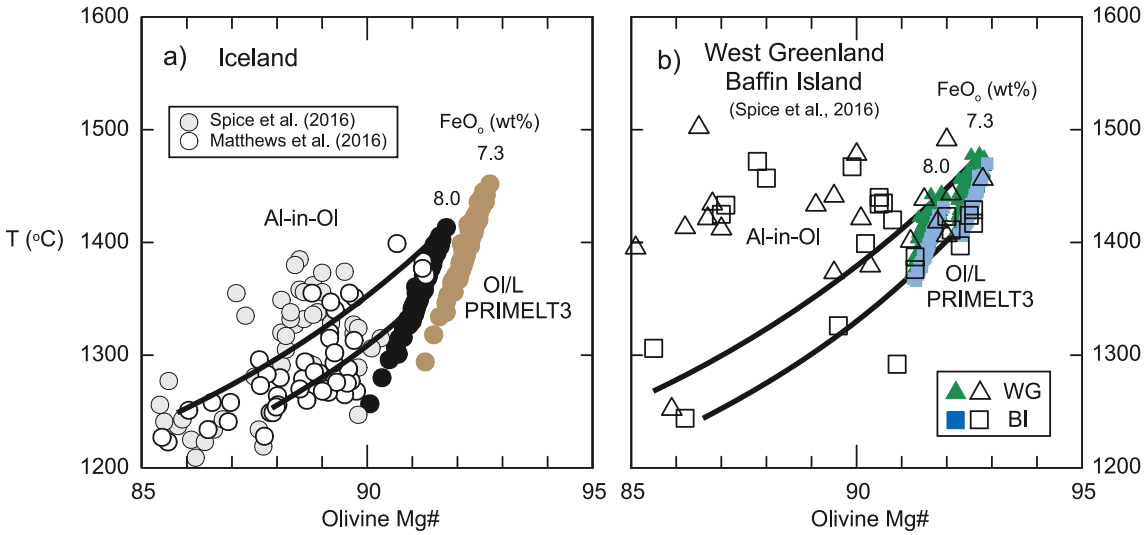

Figure 10. A comparison of Al-in-Ol and Ol/L PRIMELT3 temperatures at 1 atm plotted against olivine Mg numbers calculated for successful primary magma solutions. PRIMELT3 Ol/L temperatures are from Equation 13 in Herzberg and Asimow (2015), reproduced as Equation 14 in this work; olivine Mg# is calculated with the Toplis (2005) model. (a) Iceland olivines in equilibrium with PRIMELT3 solutions were obtained from a peridotite source having FeO$_o$ = 8.0% (black circles) and 7.3 wt.% (brown circles). The two black curves are example olivine compositions that would crystallize at the temperatures shown by olivine crystallization from the primary magmas, crystal lines of descent. (b) Older Paleocene West Greenland and Baffin Island picrites are from the ancestral Icelandic mantle plume, with olivines from primary magma solutions obtained from data reported by Larsen and Pedersen (2009) and Starkey et al. (2009), respectively. Note that PRIMELT3 solutions are most similar to Al-in-Ol data of Spice et al. (2016) in the case of a depleted peridotite source having 7.3% FeO.

Spandler & O'Neill, 2010). This tendency is much more conspicuous in a compilation of Al-in-Ol temperature and Mg# of olivines from picrites from West Greenland and Baffin Island, thought to be products of the ancestral Iceland plume (Figure 10b). Maximum PRIMELT3-P solutions for primary magma olivine liquidus temperature and Mg# for this suite are ~1480°C and 92.7, respectively, in excellent agreement with Al-in-Ol temperatures at the high end of observed olivine *Mg#*. But the data reveal a lack of correlation between temperature and Mg# at lower Mg#, which most likely reflects diffusive resetting of Fe-Mg in many samples.

The independent results from PRIMELT3 and Al-in-Ol temperatures concur that the Icelandic mantle plume is thermally heterogeneous in space and time. The agreement between these methods suggests that the apparent range in PRIMELT3-P T_P values among Iceland samples (similar to ranges found in other localities; Herzberg & Asimow, 2008; Herzberg & Gazel, 2009) is not an artifact but the consequence of real variations in temperature in the source. This result should come as no surprise because a hot mantle plume rising through cooler ambient mantle is expected to be hottest in the core and coolest at the periphery. This behavior is seen in numerical models of plume ascent (Farnetani & Samuel, 2005; Ribe & Christensen, 1999; Sleep, 2008).

4.5. The Meaning of Primary Magmatic Final Melting Pressure P_f and Significance of Variable Mantle Potential Temperature

The wide range of final melting pressures P_f (and corresponding depths) for Iceland (Figure 8) are, like the range of T_P estimates, a record of primary magma heterogeneity. If the minimum pressures represent the Moho, where decompression melting stops (Figure 8), then what is the meaning of the higher values of P_f? Early models of crust production by fractional melting assumed that instantaneous fractional melts mix perfectly during transport in a diffuse low porosity peridotite matrix, without reaction with the matrix (e.g., Langmuir et al., 1992). If this is true, then it is difficult to imagine how a primary magma with elevated P_f could survive the effects of mixing during transport. But subsequent work on melt transport indicates that both MORB and OIB melting regimes feature a transition from dominantly diffuse flow in a low porosity matrix to dominantly focused flow in high-flux melt channels (e.g., Aharonov et al., 1995; Kelemen et al., 1995; Stracke, 2021). Such channelized flow can prevent mixing with later increments of melt production and preserve high-pressure geochemical signatures (Lambart et al., 2019; Spiegelman & Kelemen, 2003). This is the model we adopt for Iceland.

10.1029/2022GC010657

Figure 11. A model for melt transport in a mantle plume. Dark dendritic forms are high flux melt channels within a low porosity peridotite matrix. Gray scaling represents mantle potential temperature variations: white is hottest at the mantle plume center; dark is coolest at the mantle plume periphery.

To explain the coexistence in the erupted suite of lavas that ceased mixing at different depths (and pressures), it seems necessary that the melt transport system contain multiple, independent channels that nucleate at different depths. Some cartoons and models of channelized melt migration systems feature such a range (Kelemen et al., 1995; Liang et al., 2010) whereas others imply that all channels nucleate at about the same depth (Aharonov et al., 1995; Hart, 1993; Keller et al., 2017). Models that feature a range of channel nucleation depths sometimes include embedded lithologic heterogeneities as nuclei for channel formation (Katz & Weatherly, 2012). We propose that the pressure at which this occurs gives a measure of meaning to magmatic pressure P_f, and that it is a pressure at which the melts "segregate" into channels. But segregation is likely imperfect, and complexities abound. Magma mixing may still occur to some extent as an individual channel receives matrix melt along its length. Channels may merge and mix the melts ascending within them. Therefore, primary magmas that record depths in the 30–90 km range (Figure 8) may be mixtures to a large degree; for example, a specific lava with a P_f solution of 60 km may not necessarily indicate the existence of a high flux channel in the melting regime below that isolates a batch of primary magma at 60 km depth. Mixing therefore obscures the meaning of a computed magmatic pressure. However, this problem does not diminish our main conclusion that melt channels are required for transport of high-pressure melts.

Figure 11 shows the branching patterns of cracks in a decaying asphalt road surface. We offer it as a qualitative analogy for the geometry of the melt migration channel network that may deliver primary magmas from the melting regime with a range of P_f signatures even though melting in the regime as a whole continues to a well-defined minimum depth. It recalls in some ways the original fractal tree model of Hart (1993), which focused on the branching properties of the network without discussing diversity among channels at a given generation of branching. Figure 11 is too simplistic to capture the physics of melt transport in a mantle plume, but it captures some aspects of geometry that seems necessary for preserving high pressure primary magma heterogeneity. Superposed on the melt channel network in Figure 11 is a gray scaling that ranges from white at the center to dark at the periphery, representing mantle plume temperatures that are highest along the axis and lowest at the periphery. Melt channels can sample hot and cold primary magmas from variable depths. The maximum mantle potential temperature in the Western Volcanic Zone of Iceland, 1520°C, could represent primary magmas that are primarily drawn into channels along the axis of the plume, whereas samples expressing lower T_P (down to 1340°C) may be drawn from channels that better sample the periphery of the plume near contact with ambient mantle or overlying lithosphere. Hence the image in Figure 11 shows at least an analogy for the coexistence of P_f and T_P heterogeneity in the products of a plume melting regime.

4.6. Effects of Lithological Heterogeneity on Magmatic Pressure Estimation

In addition to variation in potential temperature across a melting regime and in the segregation depths of melt extraction channels, both of which create heterogeneity among erupted samples that PRIMELT3-P is well-equipped to resolve, there is heterogeneity among samples due to lithological heterogeneity in the source, which raises several challenges.

Shorttle et al. (2014) reported a wide range of CaO contents for primitive Icelandic lavas as well as negative correlation between CaO and both Nb/Zr and $^{87}Sr/^{86}Sr$. As discussed more fully below, they identified an enriched component having low CaO and Nb/Zr > 0.125, and a depleted component with high CaO and Nb/Zr < 0.05. Out of 305 samples in this database, PRIMELT3-P provides only 93 successful solutions that are consistent with the calibration from fertile peridotite KR-4003; P_f values are ~1–3 GPa (Figures 8 and 12a). About one-third of the samples in the database have low CaO contents and PRIMELT3-P flags them as faux solutions with either the pyroxenite source using filter (Equation 16) or the "augite fractionation" filter (Figure 2).

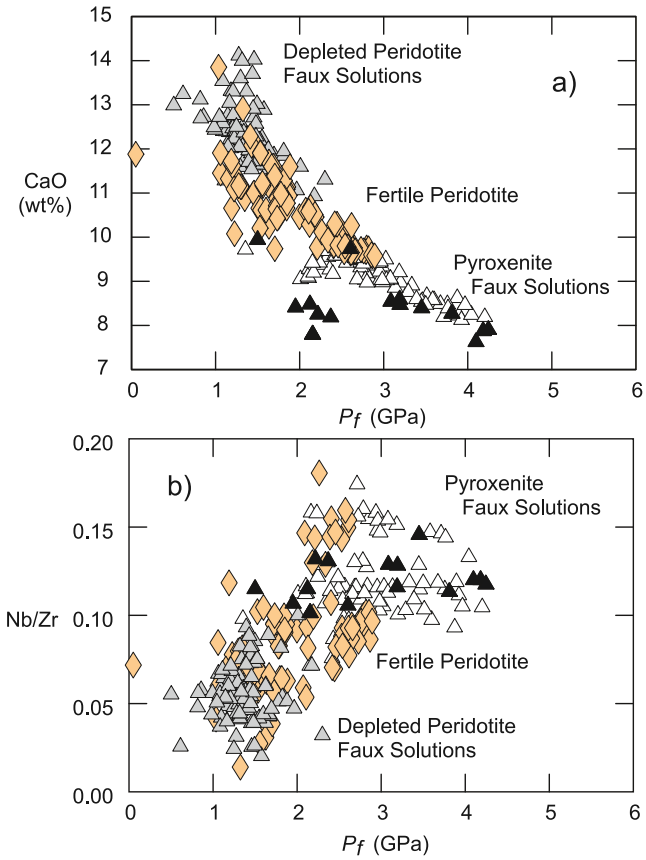

Figure 12. The effect of source lithology on computed pressures of melting calculated with PRIMELT3-P on Icelandic basalts with $FeO/FeO_T = 0.85$ using the database of Shorttle et al. (2014). Black filled triangles are solutions with CaO contents lower than those of Equation 16 and which plot below the red line in Figure 2; these are identified as a low-CaO pyroxenite source, and the solutions are false, or faux, because they were calibrated for fertile peridotite source melting, not pyroxenite melting. White filled triangles are low CaO solutions that plot in the narrow space between peridotite source melts and the red line in Figure 2 and identified as "Augite Fractionation from Peridotite Melts"; these have similar Nb/Zr as pyroxenite-source melts and augite fractionation from a peridotite source melt cannot elevate Nb/Zr. Gray filled triangles are solutions with CaO contents that are higher than those of Equation 17; these likely formed by melting depleted mantle peridotite, and the solutions for pressure are also faux because they were calibrated for fertile peridotite source melting, not depleted peridotite melting.

Evidence in support of a role for pyroxenite is provided by their high Nb/Zr (Figure 12b), a signature of enriched recycled crust in the source (Shorttle et al., 2014; Shorttle & Maclennan, 2011). Application of PRIMELT3-P to these low-CaO lavas yields faux pressures that are too high, up to 4.2 GPa for Iceland. These erroneously high faux pressures result in mantle potential temperatures T_P of about 1600°C, that is, 80°C too high.

Mapping the Icelandic samples assigned to peridotite and pyroxenite melting based on CaO versus MgO (Equation 16) into Nb/Zr space suggests that Nb/Zr ~ 0.10 roughly divides fertile peridotite source lavas below from low-CaO melt pyroxenite sources above (Figure 12b). A subset of Icelandic samples have CaO contents that are too high to be consistent with normal fertile peridotite source melting (Figure 12a). These are flagged by PRIMELT3-P as compromised by augite accumulation, based on Equation 17. However, these samples are also characterized by extremely low Nb/Zr (Figure 12b), and this cannot be a signature of augite accumulation. These high-CaO lavas are also unlikely to be high-CaO pyroxenite source melts because they are depleted in trace elements, Nb/Zr is low (Figure 12b) and $^{143}Nd/^{144}Nd$ = 0.5130 5–0.51315 (http://georoc.mpch-mainz.gwdg.de/georoc/), similar to depleted abyssal peridotite (Stracke et al., 2019). Instead, the evidence from experimental petrology is that these high-CaO lavas melted from a depleted peridotite source. Counterintuitively, experimental melts on depleted peridotite compositions that are deficient in CaO can yield high-CaO melts (Laporte et al., 2004; Wasylenki et al., 2003), similar in composition to many of the high-CaO Icelandic lavas. This is evidence supporting a depleted component in the Icelandic mantle plume (Fitton, Godard, & et al., 2004).

The origin of high-CaO lavas from Iceland is relevant to the question of whether there is harzburgite in the Icelandic mantle plume and, if so, whether it is too refractory to melt (Brown et al., 2020; Shorttle et al., 2020). The most depleted peridotite composition that has been studied experimentally is "depma," a harzburgite with 3.5% Cpx (Laporte et al., 2004). Some of the experimental melts of this composition have CaO contents similar to some of the highest CaO lavas from Iceland. Interpretation the high-CaO Icelandic lavas as products of melting such depleted harzburgite evidently implies the presence of harzburgite as a distinct lithology in the Icelandic mantle plume (Shorttle et al., 2014, 2020), but it is not consistent with the conclusion that such harzburgite does not melt (Shorttle et al., 2014). Furthermore, there are successful PRIMELT3 solutions that plot in the field of melts coexisting with residual harzburgite (Figure 8). In contrast, no role for harzburgite is possible in the model of Krein et al. (2021) because the very definition of a primary magmas in their model requires equilibrium with the assemblage Olivine + Orthopyroxene + Augite ± Plagioclase ± Spinel ± Garnet.

There are some outlying fertile peridotite solutions with Nb/Zr > 0.10, in the range expected for pyroxenites according to PRIMELT3-P (Figure 12b). These may reflect important limitations in the PRIMELT3-P CaO-based source lithology filter (Section 2.6), that is, these high-Nb/Zr lavas may be derived from pyroxenite sources and are erroneously identified by PRIMELT3-P as peridotite-source solutions. Alternatively, these outliers may represent melts derived from peridotite that were fertilized by impregnation of pyroxenite source melts, elevating Nb/Zr without strongly altering the peridotite modal mineralogy.

Shorttle and Maclennan (2011) proposed an enriched source component that was produced by the fertilization of depleted peridotite with ~33% MORB, similar to KG2 of Kogiso et al. (1998), which has 28.83% MgO and may be considered an olivine-rich pyroxenite. They identified their end-member enriched basalt with the partial melting experiment KH-26 of Kogiso et al. (1998) at 3 GPa, which has 15.57% MgO and 9.4% CaO. Shorttle et al. (2014) subsequently proposed that melts like KG2 had Nb/Zr > 0.125 and that it mixed with

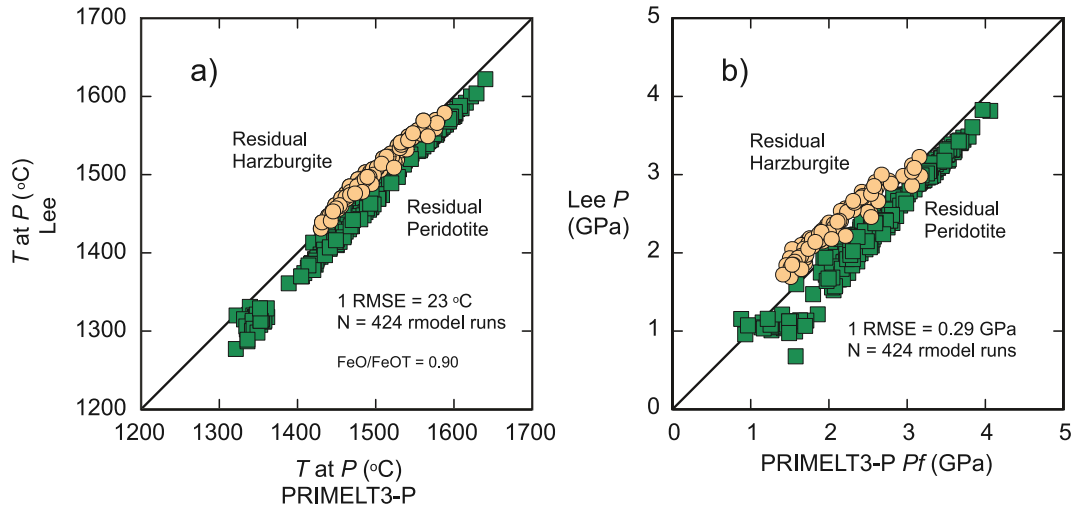

Figure 13. Magmatic temperatures and pressures of primary magmas of fertile peridotite calculated from PRIMELT3-P and FractionatePT3 (Lee et al., 2009).

melts of depleted peridotite, high in CaO and with Nb/Zr < 0.05, prior to eruption to produce the full Nb/Zr array. However, this model is problematic because the depleted and enriched end-members and their mixed melts have Al_2O_3 contents that are lower than a large population of Icelandic basalts and their primary magmas as discussed in in Supporting Information S1. Also, trace element olivine chemistry shows that peridotite is the dominant source lithology for Icelandic basalts from Snæfellsnes, the Northern Rift Zone and the Reykjanes part of the Western Rift Zone (Rasmussen et al., 2020) for which we have successful PRIMELT3 solutions. However, evidence for mixed pyroxenite and peridotite source melts is found in the South Iceland Volcanic Zone and Tertiary lavas in the west (Rasmussen et al., 2020). The implication is that variations in Nb/Zr reflect a significant role of variable fertilization of peridotite from partial melts of pyroxenite. However, we concur that mixing of peridotite- and pyroxenite-source melts may have occurred as both are identified by their calcium contents as discussed in Section 2.6. For mixed melts, PRIMELT3-P mantle potential temperatures and final melting pressures will be erroneous to the extent determined by the mass proportions and compositional differences between peridotite and pyroxenite melts in the mixture.

5. A Deeper Comparison of PRIMELT3-P and FractionatePT3 (Lee et al., 2009)

Having discussed in detail the Iceland and Hawai'i case studies, let us now compare thermobarometric results for a broader sampling of basalts from terrains around that world that feature lavas primitive enough to have only fractionated olivine. The set of 424 successful primary magma solutions considered includes lavas from post-shield Mauna Kea volcano (database in Herzberg and Asimow (2008)), West Greenland (Larsen & Pedersen, 2009), Baffin Island (Starkey et al., 2009), the Galapagos archipelago [GEOROC: http://georoc.mpch-mainz.gwdg.de], and the Azores [GEOROC]. All temperatures and pressures are computed with $FeO/FeO_T = 0.90$ for purposes of internal consistency. Only primary magma solutions that pass all the PRIMELT3-P quality filters (pyroxenite melting, augite fractionation/accumulation, and volatile peridotite melting) are considered; each solution is compatible with extraction from a peridotite or harzburgite residue, the basis for the PRIMELT calibration. FractionatePT3 was then applied to each of these successful PRIMELT3-P solutions in order to compare pressures and temperature obtained from the two calibrations.

Temperatures obtained by PRIMELT3-P and FractionatePT3 agree with a root-mean square error (RMSE) of ±23°C (Figure 13a) and pressures agree with a RMSE of ±0.29 GPa (Figure 13b). The agreement is substantially better for the subset of solutions identified by PRIMELT3-P as having harzburgite residues. The overall agreement in pressure estimates is unexpected, given that the two methods are independent calibrations based on different melting models — batch melting in FractionatePT3 and accumulated polybaric fractional melting in PRIMELT3-P. However, this result was anticipated by Asimow and Longhi (2004) who showed that a polybaric accumulated fractional melt can coincidentally display the properties of multiple saturation at a specific pressure

that is characteristic of a single batch primary melt in equilibrium with the mantle. The Siqueiros MORB samples, for example, yield a mean P_f of 1.4 GPa from PRIMELT3-P and a mean pressure of 1.3 GPa from FractionatePT3 (using a modestly FeO-depleted source composition). This is in excellent agreement with liquidus experiments on primitive Siqueiros glass samples which show multiple saturation with olivine, opx, cpx, and possibly spinel at 1.2–1.3 GPa (Wendlandt & Ridley, 1994).

The ±0.20 GPa 1σ uncertainty in FractionatePT3 (Lee et al., 2009) and ±0.29 GPa RMSE difference from PRIMELT3-P P_f suggests that the two methods have comparable uncertainties. There is no clear advantage in using PRIMELT3-P instead of FractionatePT3. Both methods yield magmatic pressures that are consistent with independent constraints on the depths to the lithosphere asthenosphere boundary below Hawai'I and the Moho below Iceland. However, the advantage of PRIMELT3-P is its ability to identify residual mineralogy and lithological heterogeneity and to generate a warning when solutions are compromised by pyroxenite in the sources. The exclusion of primary magma solutions that have been compromised by pyroxenite is expected to greatly reduce the wide temperature and pressure arrays that are typically calculated with FractionatePT3 (Lee et al., 2009).

6. Conclusions

This paper reports new software called PRIMELT3-P, released in both Excel and Python versions, for computing and understanding pressure range for derivation of primary magmas of basalts. It is a calibration of a forward model of adiabatic decompression fractional melting of fertile mantle peridotite in one dimension (up a vertical streamline, appropriate to a cylindrical column). It computes initial and final melting pressure, the MgO content of the primary melt and the Mg# of the liquidus olivine, mantle potential temperature, and olivine liquidus temperatures at various pressures. We illustrate the utility of PRIMELT3-P by applying it to databases of lava compositions from Hawai'i and Iceland, where there are independent geophysical constraints on the depths to the melting regimes.

The underlying assumptions behind PRIMELT3-P differ from those leading to FractionatePT3 (Lee et al., 2009). The former assumes polybaric fractional melting whereas the latter assumes batch melting. Nevertheless, application of both methods to primary magma solutions from PRIMELT3 yields calculated pressures that agree to within ±0.29 GPa RMSE, as anticipated by Asimow and Longhi (2004). The advantage of PRIMELT3-P over FractionatePT3 is therefore not in the accuracy or precision of its pressure estimates. Instead, it lies in the self-consistent method by which PRIMELT3 identifies the primary melt and in its ability identify lithological heterogeneity and distinguish peridotite sources (where the models are appropriate) from pyroxenite sources (where they are not). Both methods can fail when applied to melts extracted from pyroxenite sources. The consequences of ignoring recycled crust in the form of pyroxenite can yield mantle potential temperature T_P and P_f from both methods can be too high by ∼100°C and 2 GPa, respectively.

For Mauna Kea, application of PRIMELT3-P and FractionatePT3 to basalts with $FeO/FeO_T = 0.90$ yield primary magma pressures that are coincident with those where there is the greatest reduction in S wave velocities inferred from receiver functions (Rychert et al., 2013). Melting pressures from PRIMELT3-P are 3.1–3.5 GPa, equivalent to depths of final melting of 100–115 km. These pressures/depths are only slightly higher than those defined by the Gutenberg Discontinuity, or LAB, for the Pacific oceanic lithospheric plate at the location of Hawai'i, consistent with models that the LAB is a barrier to vertical mantle plume transport and melting. Both PRIMELT3-P and FractionatePT3 agree that mantle potential temperatures below Hawai'i are 1520–1560°C, 200°C higher than for Siqueiros MORB.

Icelandic peridotite-source primary magma compositions are more heterogeneous than those for Hawai'i, resulting in a greater range of depths/pressures and mantle potential temperatures. Minimum pressures are best matched with the depth to the seismic Moho when the primary magmas are computed from basalts that have $FeO/FeO_T = 0.85$. Pressures range from 1 to 3 GPa, and mantle potential temperature T_P varies from 1340 to 1520°C. Similarly, PRIMELT3-P predicts a large range of olivine liquidus temperatures at 1 atm, and they are similar to those independently obtained from Al-in-Olivine thermometry.

The meaning of primary magma pressure is clarified but complex. There is typically a range of pressures in each locality, with minima that are coincident with independent geophysical constraints on the depths to the top of the melting regime. However, the range of final melting pressures may be in part a record of magma transport, mixing and variability in the transition from diffuse porous flow to channelized flow. Computed temperature and

pressure arrays arising from heterogeneous peridotite-source primary magmas may reflect melt transport and mixing in a thermally zoned mantle plume with a complex network of branching melt channels that nucleate over a range of depths.

Data Availability Statement

Whole rock basalt data from HSDP2 core samples of Mauna Kea (DeFelice et al., 2019) and their successful PRIMELT3-P solutions are provided in Table S1. Whole rock basalt data from Iceland (Shorttle et al., 2014) and their successful PRIMELT3-P solutions are archived in Table S2 in Supporting Information S1. This data set is also available at the Caltech data repository https://doi.org/10.22002/yfn7a-90x53. Both the Excel and GUI version of PRIMELT3-P are maintained on Gitlab and can be downloaded for free from https://gitlab.com/primelt_software/primelt3-p and from a Caltech data repository https://doi.org/10.22002/6te59-vad07. After downloading the Excel version, the following warning will appear: SECURITY RISK Microsoft has blocked macros from running because the source of this file is untrusted. Macros can be unblocked in one of two ways: (a) save the workbook, close it, and then open it, (b) close the workbook, right click on the workbook, select Properties, select General tab, select Security, check Unblock, press Apply.

Acknowledgments
We are grateful to Shichun Huang, Oliver Shorttle, Sarah Lambart, Godfrey Fitton and Catherine Rychert for generously providing databases and thoughtful discussions. Juan David Hernández-Montenegro acknowledges support by a grant from the Fulbright foundation. PDA acknowledges support from NSF award 1947616. We are grateful to two anonymous reviewers for their thoughtful comments.

References

Aharonov, E., Whitehead, J. A., Kelemen, P. B., & Spiegelman, M. (1995). Channeling instability of upwelling melt in the mantle. *Journal of Geophysical Research*, *100*(B10), 20433–20450. https://doi.org/10.1029/95jb1307

Ahern, J. L., & Turcotte, D. (1979). Magma migration beneath an ocean ridge. *Earth and Planetary Science Letters*, *46*(1), 115–122. https://doi.org/10.1016/0012-821x(79)90113-4

Albarède, F. (1992). How deep do common basaltic magmas form and differentiate? *Journal of Geophysical Research*, *97*, 10997–11009.

Arevalo, R., Jr., & McDonough, W. F. (2010). Chemical variations and regional diversity observed in MORB. *Chemical Geology*, *271*(1–2), 70–85. https://doi.org/10.1016/j.chemgeo.2009.12.013

Asimow, P. D. (2022). The petrological consequences of the estimated oxidation state of primitive MORB glass. In R. Moretti & D. R. Neuville (Eds.), *Magma redox chemistry*, (Vol. 266, pp. 139–154). Geophysical Monograph Series

Asimow, P. D., Hirschmann, M. M., & Stolper, E. M. (1997). An analysis of variations in isentropic melt productivity. *Philosophical Transactions of the Royal Society of London, Series A*, *355*(1723), 255–281. https://doi.org/10.1098/rsta.1997.0009

Asimow, P. D., Hirschmann, M. M., & Stolper, E. M. (2001). Calculation of peridotite partial melting from thermodynamic models of minerals and melts, IV. Adiabatic decompression and the composition and mean properties of mid-ocean ridge basalts. *Journal of Petrology*, *42*(5), 963–998. https://doi.org/10.1093/petrology/42.5.963

Asimow, P. D., & Longhi, J. (2004). The significance of multiple saturation points in the context of polybaric near-fractional melting. *Journal of Petrology*, *45*(12), 2349–2367. https://doi.org/10.1093/petrology/egh043

Beattie, P. (1993). Olivine-melt and orthopyroxene-melt equilibria. *Contributions to Mineralogy and Petrology*, *115*(1), 103–111. https://doi.org/10.1007/bf00712982

Berry, A. J., Stewart, G. A., O'Neill, H. S., Mallmann, G., & Mosselmans, J. F. W. (2018). A re-assessment of the oxidation state of iron in morb glasses. *Earth and Planetary Science Letters*, *483*, 114–123. https://doi.org/10.1016/j.epsl.2017.11.032

Bézos, A., Guivela, C., La, C., Fougeroux, T., & Humler, E. (2021). Unraveling the confusion over the iron oxidation state in MORB glasses. *Geochimica et Cosmochimica Acta*, *293*, 28–39. https://doi.org/10.1016/j.gca.2020.10.004

Breddam, K., Kurz, M. D., & Storey, M. (2000). Mapping out the conduit of the iceland mantle plume with helium isotopes. *Earth and Planetary Science Letters*, *176*(1), 45–55. https://doi.org/10.1016/s0012-821x(99)0031-1

Brounce, M., Stolper, E., & Eiler, J. (2017). Redox variations in Mauna Kea lavas, the oxygen fugacity of the Hawai`ian plume, and the role of volcanic gases in Earth's oxygenation. *Proceedings of the National Academy of Sciences*, *114*(34), 8997–9002. https://doi.org/10.1073/pnas.1619527114

Brown, E. L., & Lesher, C. E. (2014). North Atlantic magmatism controlled by temperature, mantle composition and buoyancy. *Nature Geoscience*, *7*(11), 820–824. https://doi.org/10.1038/ngeo2264

Brown, E. L., Petersen, K. D., & Lesher, C. E. (2020). Markov chain Monte Carlo inversion of mantle temperature and source composition, with application to Reykjanes Peninsula, Iceland. *Earth and Planetary Science Letters*, *532*, 116007. https://doi.org/10.1016/j.epsl.2019.116007

Coogan, L., Saunders, A., & Wilson, R. (2014). Aluminum-in-olivine thermometry of primitive basalts: Evidence of an anomalously hot mantle source for large igneous provinces. *Chemical Geology*, *368*, 1–10. https://doi.org/10.1016/j.chemgeo.2014.01.004

Coogan, L. A., & O'Hara, M. J. (2015). MORB differentiation: In situ crystallization in replenished–tapped magma chambers. *Geochimica et Cosmochimica Acta*, *158*, 147–161. https://doi.org/10.1016/j.gca.2015.03.010

Cottrell, E., Birner, S. K., Brounce, M., Davis, F. A., Waters, L. E., & Kelley, K. A. (2022). Oxygen fugacity across tectonic settings. In R. Moretti & D. R. Neuville (Eds.), *Magma redox chemistry*, (Vol. 266, pp. 33–61). Geophysical Monograph Series.

Davis, F. A., Hirschmann, M. M., & Humayun, M. (2011). The composition of the incipient partial melt of garnet peridotite at 3 GPa and the origin of OIB. *Earth and Planetary Science Letters*, *308*(3–4), 380–390. https://doi.org/10.1016/j.epsl.2011.06.008

DeFelice, C., Mallick, S., Saal, A. E., & Huang, S. (2019). An isotopically depleted lower mantle component is intrinsic to the Hawai`ian mantle plume. *Nature Geoscience*, *12*(6), 487–492. https://doi.org/10.1038/s41561-019-0348-0

Farnetani, C. G., & Samuel, H. (2005). Beyond the thermal plume paradigm. *Geophysical Research Letters*, *32*(7), L07311. https://doi.org/10.1029/2005GL022360

Fitton, G. J., & Godard, M. (2004). Origin and evolution of magmas on the Ontong Java Plateau. In J. G. Fitton (Ed.), *Origin and evolution of the Ontong Java Plateau*, *151–178* (Vol. 229). The Geological Society.

Gaborieau, M., Laubier, M., Bolfan-Casanova, N., McCammon, C. A., Vantelon, D., Chumakov, A. I., et al. (2020). Determination of $Fe^{3+}/\Sigma Fe$ of olivine-hosted melt inclusions using Mössbauer and XANES spectroscopy. *Chemical Geology*, *547*, 119646. https://doi.org/10.1016/j.chemgeo.2020.119646

Gavrilenko, M., Herzberg, C., Vidito, C., Carr, M. J., Tenner, T., & Ozerov, A. (2016). A calcium-in-olivine geohygrometer and its application to subduction zone magmatism. *Journal of Petrology*, *57*(9), 1811–1832. https://doi.org/10.1093/petrology/egw06

Ghiorso, M. S., Hirschmann, M. M., Reiners, P. W., & Kress, V. C., III. (2002). The pMELTS: A revision of MELTS for improved calculation of phase relations and major element partitioning related to partial melting of the mantle to 3 GPa. *Geochemistry, Geophysics, Geosystems*, *3*(5), 1–35. https://doi.org/10.1029/2001GC000217

Ghiorso, M. S., & Sack, R. O. (1995). Chemical mass transfer in magmatic processes IV. A revised and internally consistent thermodynamic model for the interpolation and extrapolation of liquid-solid equilibria in magmatic systems at elevated temperatures and pressures. *Contributions to Mineralogy and Petrology*, *119*(2–3), 197–212. https://doi.org/10.1007/bf00307281

Gualda, G. A. R., Ghiorso, M. S., Lemons, R. V., & Carley, T. L. (2012). Rhyolite-MELTS: A modified calibration of MELTS optimized for silica-rich, fluid-bearing magmatic systems. *Journal of Petrology*, *53*(5), 875–890. https://doi.org/10.1093/petrology/egr080

Haase, K. (1996). The relationship between the age of the lithosphere and the composition of oceanic magmas: Constraints on partial melting, mantle sources and the thermal structure of the plates. *Earth and Planetary Science Letters*, *144*(1–2), 75–92. https://doi.org/10.1016/0012-821x(96)00145-8

Hart, S. R. (1993). Equilibration during mantle melting: A fractal tree model. *Proceedings of the National Academy of Sciences*, *90*(24), 11914–11918. https://doi.org/10.1073/pnas.90.24.11914

Hartley, M. E., Shorttle, O., Maclennan, J., Moussallam, Y., & Edmonds, M. (2017). Olivine-hosted melt inclusions as an archive of redox heterogeneity in magmatic systems. *Earth and Planetary Science Letters*, *479*, 192–205.

Harðardóttir, S., Halldórssona, S. A., & Hilton, D. R. (2018). Spatial distribution of helium isotopes in Icelandic geothermal fluids and volcanic materials with implications for location, upwelling and evolution of the Icelandic mantle plume. *Chemical Geology*, *480*, 12–27. https://doi.org/10.1016/j.chemgeo.2017.05.012

Hays, M. R. (2004). *Intra-transform volcanism along the Siqueiros fracture zone 8° 20'N - 8°30'N, East Pacific Rise*. Master of Science Thesis. University of Florida.

Helz, R. T., Cottrell, E., Brounce, M. N., & Kelley, K. A. (2017). Olivine-melt relationships and syneruptive redox variations in the 1959 eruption of Kılauea Volcano as revealed by XANES. *Journal of Volcanology and Geothermal Research*, *333–334*, 1–14. https://doi.org/10.1016/j.jvolgeores.2016.12.006

Herzberg, C. (2004). Geodynamic information in peridotite petrology. *Journal of Petrology*, *45*(12), 2507–2530. https://doi.org/10.1093/petrology/egh039

Herzberg, C. (2006). Petrology and thermal structure of the Hawai`ian plume from Mauna Kea volcano. *Nature*, *444*, 605–609.

Herzberg, C. (2011). Identification of source lithology in the Hawai`ian and Canary Islands: Implications for origins. *Journal of Petrology*, *52*(1), 113–146. https://doi.org/10.1093/petrology/egq075

Herzberg, C. (2022). Understanding the paleoproterozoic circum-superior large igneous province constrains the thermal properties of Earth's mantle through time. *Precambrian Research*, *375*, 106671. https://doi.org/10.1016/j.precamres.2022.106671

Herzberg, C., & Asimow, P. D. (2008). Petrology of some oceanic island basalts: PRIMELT2.XLS software for primary magma calculation. *Geochemistry, Geophysics, Geosystems*, *8*(9), Q09001. https://doi.org/10.1029/2008GC002057

Herzberg, C., & Asimow, P. D. (2015). PRIMELT3 MEGA.XLSM software for primary magma calculation: Peridotite primary magma MgO contents from the liquidus to the solidus. *Geochemistry, Geophysics, Geosystems*, *16*(2), 563–578. https://doi.org/10.1002/2014GC005631

Herzberg, C., Condie, K., & Korenaga, J. (2010). Thermal evolution of the Earth and its petrological expression. *Earth and Planetary Science Letters*, *292*(1–2), 79–88. https://doi.org/10.1016/j.epsl.2010.01.022

Herzberg, C., & Gazel, E. (2009). Petrological evidence for secular cooling in mantle plumes. *Nature*, *458*(7238), 619–622. https://doi.org/10.1038/nature07857

Herzberg, C., & O'Hara, M. J. (2002). Plume-associated ultramafic magmas of Phanerozoic age. *Journal of Petrology*, *43*(10), 1857–1883. https://doi.org/10.1093/petrology/43.10.1857

Herzberg, C., Raterron, P., & Zhang, J. (2000). New experimental observations on the anhydrous solidus for peridotite KLB-1. *Geochemistry, Geophysics, Geosystems*, *1*(11). https://doi.org/10.1029/2000GC000089

Herzberg, C., & Rudnick, R. (2012). Formation of cratonic lithosphere: An integrated thermal and petrological model. *Lithos*, *149*, 4–15. https://doi.org/10.1016/j.lithos.2012.01.010

Herzberg, C., & Zhang, J. (1996). Melting experiments on anhydrous peridotite KLB-1: Compositions of magmas in the upper mantle and transition zone. *Journal of Geophysical Research*, *101*(B4), 8271–8295. https://doi.org/10.1029/96jb00170

Howarth, G. H., & Harris, C. (2017). Discriminating between pyroxenite and peridotite sources for continental flood basalts (CFB) in southern Africa using olivine chemistry. *Earth and Planetary Science Letters*, *475*, 143–151. https://doi.org/10.1016/j.epsl.2017.07.043

Huang, S., & Humayun, M. (2016). Petrogenesis of high-CaO lavas from Mauna Kea, Hawai`i: Constraints from trace element abundances. *Geochimica et Cosmochimica Acta*, *185*, 198–215. https://doi.org/10.1016/j.gca.2016.03.039

Jennings, E. S., & Holland, T. J. B. (2015). A simple thermodynamic model for melting of peridotite in the system NCFMASOCr. *Journal of Petrology*, *56*(5), 869–892. https://doi.org/10.1093/petrology/egv020

Katz, R. F., & Weatherly, S. M. (2012). Consequences of mantle heterogeneity for melt extraction at mid-ocean ridges. *Earth and Planetary Science Letters*, *335–336*, 226–237. https://doi.org/10.1016/j.epsl.2012.04.042

Kelemen, P. B., Shimizu, N., & Salters, V. J. M. (1995). Extraction of mid-ocean-ridge basalt from the upwelling mantle by focused flow of melt in dunite channels. *Nature*, *375*(6534), 747–753. https://doi.org/10.1038/375747a0

Keller, T., Katz, R. F., & Hirschmann, M. M. (2017). Volatiles beneath mid-ocean ridges: Deep melting, channelised transport, focusing, and metasomatism. *Earth and Planetary Science Letters*, *464*, 55–68. https://doi.org/10.1016/j.epsl.2017.02.006

Kinzler, R. J. (1997). Melting of mantle peridotite at pressures approaching the spinel to garnet transition: Application to mid-ocean ridge basalt petrogenesis. *Journal of Geophysical Research*, *102*(B1), 853–874. https://doi.org/10.1029/96jb00988

Klemme, S., & O'Neill, H. S. C. (2000). The near-solidus transition from garnet lherzolite to spinel lherzolite. *Contributions to Mineralogy and Petrology*, *138*(3), 237–248. https://doi.org/10.1007/s004100050560

Kogiso, T., Hirose, K., & Takahashi, E. (1998). Melting experiments on homogeneous mixtures of peridotite and basalt: Application to the genesis of ocean island basalts. *Earth and Planetary Science Letters*, *162*(1–4), 45–61. https://doi.org/10.1016/s0012-821x(98)00156-3

Kogiso, T., Hirschmann, M. M., & Pertermann, M. (2004). High-pressure partial melting of mafic lithologies in the mantle. *Journal of Petrology*, *45*(12), 2407–2422. https://doi.org/10.1093/petrology/egh057

Krein, S. B., Molitor, Z. J., & Grove, T. L. (2021). *ReversePetrogen*: A multiphase dry reverse fractional crystallization mantle melting thermobarometer applied to 13, 589 mid-ocean ridge basalt glasses. *Journal of Geophysical Research: Solid Earth*, *126*(8), e2020JB021292. https://doi.org/10.1029/2020JB021292

Lambart, S., Baker, M. B., & Stolper, E. M. (2016). Role of pyroxenite in basalt genesis: Melt-PX, a melting parameterization for mantle pyroxenites at 0.9-5 GPa. *Journal of Geophysical Research – Solid Earth*, *121*(8), 5708–5735. https://doi.org/10.1002/2015JB012762

Lambart, S., Koornneef, J. M., Millet, M.-A., Davies, G., Cook, M., & Lissenberg, C. J. (2019). A highly heterogeneous depleted mantle recorded in the lower oceanic crust. *Nature Geoscience*, *12*(6), 482–486. https://doi.org/10.1038/s41561-019-0368-9

Lambart, S., Laporte, D., & Schiano, P. (2009). An experimental study of pyroxenite partial melts at 1 and 1.5 GPa: Implications for the major-element composition of midocean ridge basalts. *Earth and Planetary Science Letters*, *288*(1–2), 335–347. https://doi.org/10.1016/j.epsl.2009.09.038

Lambart, S., Laporte, D., & Schiano, P. (2013). Markers of the pyroxenite contribution on the major-element compositions of oceanic basalts: Review of the experimental constraints. *Lithos*, *160*, 14–36. https://doi.org/10.1016/j.lithos.2012.11.018

Langmuir, C. H., Klein, E. M., & Plank, T. (1992). Petrological systematics of mid-ocean ridge basalts: Constraints on melt generation beneath ocean ridges. In J. P. Morgan, D. K. Blackman, & J. M. Sinton (Eds.), *Mantle flow and melt generation at mid-ocean ridges*, *Geophysical monograph series* (Vol. 71, pp. 183–280). AGU.

Laporte, D., Toplis, M. J., Seyler, M., & Devidal, J.-L. (2004). A new experimental technique for extracting liquids from peridotite at very low degrees of melting: Application to partial melting of depleted peridotite. *Contributions to Mineralogy and Petrology*, *146*(4), 463–484. https://doi.org/10.1007/s00410-003-0509-3

Larsen, L. M., & Pedersen, A. K. (2009). Petrology of the Paleocene picrites and flood basalts on Disko and Nuussuaq, West Greenland. *Journal of Petrology*, *50*(9), 1667–1711. https://doi.org/10.1093/petrology/egp048

Lee, C.-T., Luffi, P., Plank, T., Dalton, H., & Leeman, W. P. (2009). Constraints on the depths and temperatures of basaltic magma generation on Earth and other terrestrial planets using new thermobarometers for mafic magmas. *Earth and Planetary Science Letters*, *279*(1–2), 20–33. https://doi.org/10.1016/j.epsl.2008.12.020

Le Roux, V., Dasgupta, R., & Lee, C.-T. A. (2011). Mineralogical heterogeneities in the Earth's mantle: Constraints from Mn, Co, Ni and Zn partitioning during partial melting. *Earth and Planetary Science Letters*, *307*(3–4), 395–408. https://doi.org/10.1016/j.epsl.2011.05.014

Liang, Y., Schiemenz, A., Hesse, M. A., Parmentier, E. M., & Hesthaven, J. S. (2010). High-porosity channels for melt migration in the mantle: Top is the dunite and bottom is the harzburgite and lherzolite. *Geophysical Research Letters*, *37*(15), L15306. https://doi.org/10.1029/2010GL044162

Longhi, J. (2002). Some phase equilibrium systematics of lherzolite melting: 1. *Geochemistry, Geophysics, Geosystems*, *3*(3), 1–33. https://doi.org/10.1029/2001GC000204

Lyubetskaya, T., & Korenaga, J. (2007). Chemical composition of Earth's primitive mantle and its variance: 1. Method and results. *Journal of Geophysical Research*, *112*(B3), B03211. https://doi.org/10.1029/2005JB004223

Maclennan, J., McKenzie, D., & Grönvold, K. (2001). Plume-driven upwelling under central Iceland. *Earth and Planetary Science Letters*, *194*(1–2), 67–82. https://doi.org/10.1016/s0012-821x(01)00553-2

Matthews, S., Shorttle, O., & Maclennan, J. (2016). The temperature of the Icelandic mantle from olivine-spinel aluminum exchange thermometry. *Geochemistry, Geophysics, Geosystems*, *17*(11), 4725–4752. https://doi.org/10.1002/2016gc006497

Matthews, S., Wong, K., Shorttle, O., Edmonds, M., & Maclennan, J. (2021). Do olivine crystallization temperatures faithfully record mantle temperature variability? *Geochemistry, Geophysics, Geosystems*, *22*(4), e2020GC009157. https://doi.org/10.1029/2020GC009157

McDonough, W. F., & Sun, S.-S. (1995). The composition of the Earth. *Chemical Geology*, *120*(3–4), 223–253. https://doi.org/10.1016/0009-2541(94)00140-4

McKenzie, D. (1984). The generation and compaction of partial melts. *Journal of Petrology*, *25*(3), 713–765. https://doi.org/10.1093/petrology/25.3.713

Moussallam, Y., Edmonds, M., Scaillet, B., Peters, N., Gennaro, E., Sides, I., & Oppenheimer, C. (2016). The impact of degassing on the oxidation state of basaltic magmas: A case study of Kılauea volcano. *Earth and Planetary Science Letters*, *450*, 317–325. https://doi.org/10.1016/j.epsl.2016.06.031

Moussallam, Y., Longpré, M.-A., McCammon, C., Gomez-Ulla, A., Rose-Koga, E. F., Scaillet, B., et al. (2019). Mantle plumes are oxidised. *Earth and Planetary Science Letters*, *527*, 115798. https://doi.org/10.1016/j.epsl.2019.115798

Niu, Y. L., Wilson, M., Humphreys, E. R., & O'Hara, M. J. (2011). The origin of intra-plate ocean island basalts (OIB): The lid effect and its geodynamic implications. *Journal of Petrology*, *52*(7–8), 1443–1468. https://doi.org/10.1093/petrology/egr030

O'Hara, M. J. (1968). Are ocean floor basalts primary magmas? *Nature*, *220*(5168), 683–686. https://doi.org/10.1038/220683a0

O'Hara, M. J., & Herzberg, C. (2002). Interpretation of trace element and isotope features of basalts: Relevance of field relations, petrology, major element data, phase equilibria, and magma chamber modeling in basalt petrogenesis. *Geochimica et Cosmochimica Acta*, *66*(12), 2167–2191. https://doi.org/10.1016/s0016-7037(02)00852-9

O'Neill, H. S. C., & Jenner, F. E. (2016). Causes of the compositional variability among ocean floor basalts. *Journal of Petrology*, *57*(11–12), 2163–2194. https://doi.org/10.1093/petrology/egx001

Palme, H., & O'Neill, H. S. C. (2003). Cosmochemical estimates of mantle composition. In H. Holland & K. K. Turekian (Eds.), *Treatise on geochemistry* (Vol. 2, 1–38). Elsevier.

Perfit, M. R., Fornari, D. J., Ridley, W. I., Kirk, P. D., Casey, J., Kastens, K. A., et al. (1996). Recent volcanism in the Siqueiros transform fault: Picritic basalts and implications for MORB magma genesis. *Earth and Planetary Science Letters*, *141*(1–4), 91–108. https://doi.org/10.1016/0012-821x(96)00052-0

Presnall, D. C., Dixon, J. R., O'Donnell, T. H., & Dixon, S. A. (1979). Generation of mid-ocean ridge tholeiites. *Journal of Petrology*, *20*(1), 3–35. https://doi.org/10.1093/petrology/20.1.3

Prytulak, J., & Elliott, T. (2007). TiO_2 enrichment in ocean island basalts. *Earth and Planetary Science Letters*, *263*(3–4), 388–403. https://doi.org/10.1016/j.epsl.2007.09.015

Putirka, K., Ryerson, F. J., Perfit, M., & Ridley, W. I. (2011). Mineralogy and composition of the oceanic mantle. *Journal of Petrology*, *52*(2), 279–313. https://doi.org/10.1093/petrology/egq080

Putirka, K. D. (2008). Thermometers and barometers for volcanic systems. *Reviews in Mineralogy and Geochemistry*, *69*(1), 61–120. https://doi.org/10.2138/rmg.2008.69.3

Rasmussen, M. B., Halldórsson, S. A., Gibson, S. A., & Guðfinnsson, G. H. (2020). Olivine chemistry reveals compositional source heterogeneities within a tilted mantle plume beneath Iceland. *Earth and Planetary Science Letters*, *531*, 116008. https://doi.org/10.1016/j.epsl.2019.116008

Rhodes, J. M., Huang, S., Frey, F. A., Pringle, M., & Xu, G. (2012). Compositional diversity of Mauna Kea shield lavas recovered by the Hawai`i Scientific Drilling Project: Inferences on source lithology, magma supply, and the role of multiple volcanoes. *Geochemistry, Geophysics, Geosystems*, *13*(3), Q03014. https://doi.org/10.1029/2011GC003812

Rhodes, J. M., & Vollinger, M. J. (2004). Composition of basaltic lavas sampled by phase-2 of the Hawai`i Scientific Drilling Project: Geochemical stratigraphy and magma types. *Geochemistry, Geophysics, Geosystems*, *5*(3), Q03G13. https://doi.org/10.1029/2002GC000434

Ribe, N. M., & Christensen, U. R. (1999). The dynamical origin of Hawaiian volcanism. *Earth and Planetary Science Letters*, *171*, 517–531.

Rychert, C. A., Laske, G., Harmon, N., & Shearer, P. M. (2013). Seismic imaging of melt in a displaced Hawai`ian plume. *Nature Geoscience*, *6*(8), 657–660. https://doi.org/10.1038/ngeo1878

Schmerr, N. (2012). The Gutenberg discontinuity: Melt at the lithosphere-asthenosphere boundary. *Science*, *335*(6075), 1480–1483. https://doi.org/10.1126/science.1215433

Shaw, D. M. (1970). Trace element fractionation during anatexis. *Geochimica et Cosmochimica Acta*, *34*(2), 237–243. https://doi.org/10.1016/0016-7037(70)90009-8

Shorttle, O., & Maclennan, J. (2011). Compositional trends of Icelandic basalts: Implications for short-length scale lithological heterogeneity in mantle plume. *Geochemistry, Geophysics, Geosystems*, *12*(11), Q11008. https://doi.org/10.1029/2011GC003748

Shorttle, O., Maclennan, J., & Lambart, S. (2014). Quantifying lithological variability in the Mantle. *Earth and Planetary Science Letters*, *395*, 24–40. https://doi.org/10.1016/j.epsl.2014.03.040

Shorttle, O., Matthews, S., & Maclennan, J. (2020). Finding harzburgite in the mantle. A comment on Brown et al. Markov chain Monte Carlo inversion of mantle temperature and source composition, with application to Reykjanes Peninsula, Iceland. *Earth and Planetary Science Letters*, *548*, 116503.

Shorttle, O., Moussallam, Y., Hartley, M. E., Maclennan, J., Edmonds, M., & Murton, B. J. (2015). Fe-XANES analyses of Reykjanes Ridge basalts: Implications for oceanic crust's role in the solid Earth oxygen cycle. *Earth and Planetary Science Letters*, *427*, 272–285. https://doi.org/10.1016/j.epsl.2015.07.017

Sleep, N. H. (2008). Channeling at the base of the lithosphere during the lateral flow of plume material beneath flow line hot spots. *Geochemistry, Geophysics, Geosystems*, *9*(8), Q08005. https://doi.org/10.1029/2008GC002090

Sobolev, A. V., Hofmann, A. W., Kuzmin, D. V., Yaxley, G., Arndt, N. T., Chung, S. L., et al. (2007). The amount of recycled crust in sources of mantle derived melts. *Science*, *316*(5823), 590–597. https://doi.org/10.1126/science.1138113

Spandler, C., & O'Neill, H. S. C. (2010). Diffusion and partition coefficients of minor and trace elements in San Carlos olivine at 1300°C with some geochemical implications. *Contributions to Mineralogy and Petrology*, *159*(6), 791–818. https://doi.org/10.1007/s00410-009-0456-8

Spiegelman, M., & Kelemen, P. B. (2003). Extreme chemical variability as a consequence of channelized melt transport. *Geochemistry, Geophysics, Geosystems*, *4*(7), 1055. https://doi.org/10.1029/2002GC000336

Starkey, N. A., Stuart, F. M., Ellam, R. M., Fitton, J. G., Basu, S., & Larsen, L. M. (2009). Helium isotopes in early Iceland plume picrites: Constraints on the composition of high $^{3}He/^{4}He$ mantle. *Earth and Planetary Science Letters*, *277*(1–2), 91–100. https://doi.org/10.1016/j.epsl.2008.10.007

Stolper, E. M., DePaolo, D. J., & Thomas, D. M. (2009). Deep drilling into a mantle plume volcano: The Hawai`i Scientific Drilling Project. *Scientific Drilling*, *7*, 4–14. https://doi.org/10.5194/sd-7-4-2009

Stolper, E. M., Sherman, S., Garcia, M., Baker, M. B., & Seaman, C. (2004). Glass in the submarine section of the HSDP2 drill core, Hilo, Hawai`i. *Geochemistry, Geophysics, Geosystems*, *5*(7), Q07G15. https://doi.org/10.1029/2003GC000553

Stracke, A. (2021). A process-oriented approach to mantle geochemistry. *Chemical Geology*, *579*, 120350. https://doi.org/10.1016/j.chemgeo.2021.120350

Stracke, A., Genske, F., Berndt, J., & Koornneef, J. M. (2019). Ubiquitous ultra-depleted domains in Earth's mantle. *Nature Geoscience*, *12*(10), 851–855. https://doi.org/10.1038/s41561-019-0446-z

Tomlinson, E., & Holland, T. J. B. (2021). A thermodynamic model for the subsolidus evolution and melting of peridotite. *Journal of Petrology*, *62*, 1–23. https://doi.org/10.1093/petrology/egab012

Toplis, M. J. (2005). The thermodynamics of iron and magnesium partitioning between olivine and liquid: Criteria for assessing and predicting equilibrium in natural and experimental systems. *Contributions to Mineralogy and Petrology*, *149*(1), 22–39. https://doi.org/10.1007/s00410-004-0629-4

Walter, M. J. (1998). Melting of garnet peridotite and the origin of komatiite and depleted lithosphere. *Journal of Petrology*, *39*(1), 29–60. https://doi.org/10.1093/petroj/39.1.29

Wasylenki, L. E., Baker, M. B., Kent, A. J. R., & Stolper, E. M. (2003). Near-solidus melting of the shallow upper mantle: Partial melting experiments on depleted peridotite. *Journal of Petrology*, *44*(7), 1163–1191. https://doi.org/10.1093/petrology/44.7.1163

Wendlandt, R. F., & Ridley, W. I. (1994). Melting phase relations of a glassy high-MgO basalt from the Siqueiros transform domain, East Pacific Rise (EPR). *EOS Transactions, American Geophysical Union*, *75*, 720.

Workman, R. K., & Hart, S. R. (2005). Major and trace element composition of the depleted MORB mantle (DMM). *Earth and Planetary Science Letters*, *231*(1–2), 53–72. https://doi.org/10.1016/j.epsl.2004.12.005

References From the Supporting Information

Arndt, N. T., Kerr, A. C., & Tarney, J. (1997). Dynamic melting in plume heads: The formation of Gorgona komatiites and basalts. *Earth and Planetary Science Letters*, *146*(1–2), 289–301. https://doi.org/10.1016/s0012-821x(96)00219-1

Baker, M. B., & Beckett, J. R. (1999). The origin of abyssal peridotites: A reinterpretation of constraints based on primary bulk compositions. *Earth and Planetary Science Letters*, *171*(1), 49–61. https://doi.org/10.1016/s0012-821x(99)00130-2

Fitton, G. J., Saunders, A. D., Kempton, P. D., & Hardarson, B. S. (2003). Does depleted mantle form an intrinsic part of the iceland plume? *Geochemistry, Geophysics, Geosystems*, *4*(3), 1032. https://doi.org/10.1029/2002GC000424

Jackson, M. G., Cabral, R. A., Rose-Koga, E. F., Koga, K. T., Price, A., Hauri, E. H., & Michael, P. (2015). Ultra-depleted melts in olivine-hosted melt inclusions from the Ontong Java Plateau. *Chemical Geology*, *414*, 124–137. https://doi.org/10.1016/j.chemgeo.2015.08.014

Jenkins, J., Maclennan, J., Green, R. G., Cottaar, S., Deuss, A. F., & White, R. S. (2018). Crustal formation on a spreading ridge above a mantle plume: Receiver function imaging of the Icelandic crust. *Journal of Geophysical Research: Solid Earth*, *123*(6), 5190–5208. https://doi.org/10.1029/2017JB015121

Jennings, E. S., Gibson, S. A., & Maclennan, J. (2019). Hot primary melts and mantle source for the Parana-Etendeka flood basalt province: New constraints from Al-in-olivine thermometry. *Chemical Geology*, *529*, 119287. https://doi.org/10.1016/j.chemgeo.2019.119287

Herzberg, C., Asimow, P. D., Arndt, N., Niu, Y., Lesher, C. M., Fitton, J. G., et al. (2007). Temperatures in ambient mantle and plumes: Constraints from basalts, picrites, and komatiites. *Geochemistry, Geophysics, Geosystems*, *8*(2). https://doi.org/10.1029/2006GC001390

Larsen, L. M., & Williamson, M.-C. (2020). Depleted and ultradepleted basalt and picrite in the Davis Strait: Paleocene volcanism associated with a transform continental margin. *Geological Magazine*, *157*(12), 1983–2003. https://doi.org/10.1017/S0016756820000175

Spice, H. E., Fitton, J. G., & Kirstein, L. A. (2016). Temperature fluctuation of the Iceland mantle plume through time. *Geochemistry, Geophysics, Geosystems*, *17*(2), 243–254. https://doi.org/10.1002/2015GC006059

Stracke, A., Snow, J. E., Hellebrand, E., von der Handt, A., Bourdon, B., Birbaum, K., & Günther, D. (2011). Abyssal peridotite Hf isotopes identify extreme mantle depletion. *Earth and Planetary Science Letters*, *308*(3–4), 359–368. https://doi.org/10.1016/j.epsl.2011.06.012

Thompson, R. N., Riches, A. J. V., Antoshechkina, P. M., Pearson, D. G., Nowell, G. M., Ottley, C. J., et al. (2007). Origin of CFB magmatism: Multi-tiered intracrustal picrite-rhyolite magmatic plumbing at Spitzkoppe, Western Namibia, during early Cretaceous Etendeka magmatism. *Journal of Petrology*, *48*(6), 1119–1154. https://doi.org/10.1093/petrology/egm012

Warren, J. M. (2016). Global variations in abyssal peridotite compositions. *Lithos*, *248–251*, 193–219. https://doi.org/10.1016/j.lithos.2015.12.023

Waterton, P., Person, D. G., Kjarsgaard, B., Hulbert, L., Locock, A., Parman, S., & David, D. (2017). Age, origin, and thermal evolution of the ultra-fresh ∼1.9 Ga Winnipegosis Komatiites, Manitoba, Canada. *Lithos*, *268–271*, 114–130. https://doi.org/10.1016/j.lithos.2016.10.033

Willig, M., Stracke, A., Beier, C., & Salters, V. J. M. (2020). Constraints on mantle evolution from Ce-Nd-Hf isotope systematics. *Geochimica et Cosmochimica Acta*, *272*, 36–53. https://doi.org/10.1016/j.gca.2019.12.029

Zhang, L., Ren, Z.-Y., Zhang, L., Wu, Y.-D., Qian, S.-P., Xia, X.-P., & Xu, Y.-G. (2021). Nature of the mantle plume under the Emeishan large igneous province: Constraints from olivine-hosted melt inclusions of the Lijiang picrites. *Journal of Geophysical Research: Solid Earth*, *126*(5), e2020JB021022. https://doi.org/10.1029/2020JB021022